Unravelling groundwater's role in soil-plant-atmosphere continuum: Integrated ecohydrological modelling approach using STEMMUS-SCOPE and MODFLOW 6

Mostafa Gomaa Daoud[1], Fakhereh (Sarah) Alidoost[2], Yijian Zeng[1], Bart Schilperoort[2], Christiaan Van der Tol[1], Maciek W. Lubczynski[1,3], Mhd Suhyb Salama[1], Eric D. Morway[4], Christian D. Langevin[5], Prajwal Khanal[1], Zengjing Song[1], Lianyu Yu[6,7], Hong Zhao[8], Gualbert Oude Essink[9,10], Victor F. Bense[11], Michiel van der Molen[8], Javier Samper[3], Zhongbo Su[1]

[1] Department of Water Resources, Faculty of Geo-Information Science and Earth Observation (ITC), University of Twente, PO Box 217, 7522 NH Enschede, The Netherlands

[2] Netherlands eScience Center, Amsterdam, 1098XH, the Netherlands

[3] Interdisciplinary Center of Chemistry and Biology (CICA), Civil Engineering School & Department, University of A Coruña, Campus Elviña s/n, 15071 A Coruña, Spain

[4] U.S. Geological Survey, Nevada Water Science Center, Carson City, NV, USA

[5] S.S. Papadopulos & Assoc., Inc., 12 Dove Lane, Saint Paul, MN, USA

[6] College of Water Resources and Architectural Engineering, Northwest Agriculture and Forestry University, Yangling, China

[7] Key Laboratory of Agricultural Soil and Water Engineering in Arid Area of Ministry of Education, Northwest Agriculture and Forestry University, Yangling, China

[8] Meteorology and Air Quality Section, Wageningen University and Research, Wageningen, The Netherlands

[9] Unit Subsurface and Groundwater Systems, Deltares, P.O. Box 85467, 3508 AL, Utrecht, The Netherlands

[10] Department of Physical Geography, Utrecht University, PO Box 80125, 3508 TC Utrecht, The Netherlands

[11] Department of Environmental Sciences, Wageningen University and Research, Wageningen, The Netherlands

Corresponding author: Mostafa Gomaa Daoud (m.g.m.daoud@utwente.nl)

Abstract

Soil-plant-atmosphere continuum (SPAC) models are commonly used to investigate various components' role(s) in ecosystem functioning. Yet, in most SPAC models, groundwater is ignored or at best represented in an over-simplified manner, leading to misunderstanding of its critical role in simulating soil-vegetation dynamics. This study investigates groundwater's role in SPAC processes, in particular, the impacts of groundwater component (mass and energy) on: 1) regulating the soil profile, in terms of moisture and temperature; 2) the dynamics of the unsaturated/saturated zones and their further impact on water fluxes; and 3) the carbon fluxes and vegetation physiological processes (i.e. root water uptake and photosynthesis reflected by fluorescence).To ~~this end~~address this, an integrated ecohydrological modelling (IEM) framework is developed by coupling the STEMMUS-SCOPE SPAC model with the MODFLOW 6 integrated hydrological model. The standalone STEMMUS-SCOPE (ST-SC) and the coupled STEMMUS-SCOPE-MODFLOW 6 (ST-SC-MF6) models were applied over an 8-year period (1 April 2016 – 31 March 2024) to three sites in the Netherlands (Loobos, Cabauw and Veenkampen). Simulated various essential variables, including soil moisture (θ), soil temperature (T_s), groundwater level (GWL), groundwater temperature (GT), evapotranspiration (ET), gross primary productivity, net ecosystem exchange (NEE), and sun-induced chlorophyll fluorescence (SIF) were then compared to corresponding in-situ observations. Performance of both ~~to evaluate the~~ ST-SC and ST-SC-MF6 ~~setups~~was evaluated using the Kling–Gupta efficiency (KGE) and the root mean square error (RMSE) metrics. Results indicated that the groundwater contribution is spatially and temporally variable. The ST-SC-MF6 showed better

agreement with observations than the ST-SC, improving the KGE values for: a) T_s (+0.29), and ET (+0.35) at Loobos, b) θ (+0.30), ET (+0.11), NEE (+0.18), and SIF (+0.15) at Cabauw, and c) θ (+0.21), and ET (+0.15) at Veenkampen. Notably, benefits of ST-SC-MF6 simulation were particularly prominent during both wet and dry periods, i.e. improving the representation of: a) the θ dynamics during wet conditions, when hydraulic connectivity between the phreatic surface and the unsaturated zone is strong; b) the root water uptake and carbon assimilation during dry periods, when shallow groundwater mitigated vegetative water stress; and c) the T_s dynamics during both wet and dry periods, influenced by both GT and GWL, and further propagated to other T_s dependent processes/variables such as canopy temperature. Overall, the proposed ST-SC-MF6 IEM helped to: (1) incorporate groundwater as a key component of the water, energy and carbon cycles; and (2) define the important role groundwater dynamics plays in the SPAC for deepening ~~our~~ the understanding of ecosystem functioning.

Short summary

Groundwater is ignored in soil-plant-atmosphere continuum (SPAC) models, potentially underestimating its impact on soil and vegetation simulation. To address this, an integrated ecohydrological model is developed by coupling a SPAC model to a hydrological model. The coupled model improved simulation of soil moisture, temperature, evapotranspiration, carbon fluxes and fluorescence. The findings highlight groundwater role in ecosystem dynamics and advance water, energy and carbon cycle modelling. ~~This study investigates the groundwater role in soil-plant-atmosphere continuum. An integrated ecohydrological modelling approach was developed by coupling STEMMUS-SCOPE to MODFLOW 6 and applied at three sites over 8 years. The coupled model improved simulations of soil moisture and temperature, evapotranspiration, carbon fluxes and fluorescence. The findings highlight the groundwater critical role in ecosystem dynamics and its contribution to advancing water, energy and carbon cycle modelling.~~

1. Introduction

The interactions among the soil, water, vegetation and atmosphere play a fundamental role in regulating ecosystem functioning. These interactions include hydrological, thermal and carbon processes that collectively shape the dynamics of the water, energy and carbon cycles. Deepening ~~our~~ the understanding of such interactions is crucial for better supporting ecosystem resilience against the adverse impact of climate change and anthropogenic activities (Chen et al., 2024; Dai et al., 2024). To assess and monitor ecosystem functioning, a range of different physical variables are recognized (Bojinski et al., 2014; GCOS, 2025). Examples of such variables, in particular the vegetation ones are: leaf area index, above- and below-ground biomass (Atkins et al., 2018; de Conto et al., 2024), gross primary productivity, net ecosystem exchange, evapotranspiration, plant phenology (Shi et al., 2023), and more recently the sun-induced chlorophyll fluorescence (SIF), which serves as a proxy for tracking the photosynthesis process (Sun et al., 2023). Additionally, other soil-related variables play a significant role in characterizing the ecosystems' functioning, i.e. soil moisture, surface and subsurface temperature, and evaporation (Bojinski et al., 2014; Zeng et al., 2019; GCOS, 2025). ~~Essential climate variables (ECVs) are globally recognized indicators that characterize the Earth's system (Bojinski et al., 2014; GCOS, 2025). Terrestrial ECVs include key indicators of vegetation status such as leaf area index, above-ground biomass, and fraction of absorbed photosynthetically active radiation. Recent studies (Baatz et al., 2021; Cupertino et al., 2024; Muise et al., 2024) have expanded beyond the traditional ECVs to include: a) productivity variables — including gross primary productivity, net ecosystem exchange, and evapotranspiration (Baatz et al., 2021); b) structure variables — including canopy height, canopy cover, and below-ground biomass ; and c) development variables — including plant phenology (start and end of growing season; and more recently the sun-induced chlorophyll fluorescence (SIF), which serves as a proxy for tracking the photosynthesis process (Sun et al., 2023). Additionally, other soil-related variables play a significant role in characterizing the ecosystems' functioning, such as soil moisture,~~

~~surface and subsurface temperature, and evaporation (Bojinski et al., 2014; Zeng et al., 2019; GCOS, 2025).~~

Soil-plant-atmosphere continuum (SPAC) models are widely used to simulate most of the aforementioned ~~ECVs~~variables. SPAC models simulate the transfer of thermal energy and mass (water and carbon) between soil~~s~~, plants (through roots, stems and leaves), and the atmosphere (Guo, 1992). Furthermore, SPAC models are capable of assimilating remote sensing information such as canopy reflectance, vegetation optical depth, and SIF (X. Yang et al., 2021). Integrating the RS data into SPAC models enables upscaling the processes from point (plant) scale to regional scales (Senf, 2022; Van Cleemput et al., 2025), allowing for predicting ecosystem responses to regional environmental changes (Dronova & Taddeo, 2022). Examples of SPAC models are the Community Land Surface (CLM5) model (Lawrence et al., 2019), the integration of Simultaneous Transfer of Energy, Mass, and Momentum in Unsaturated Soil (STEMMUS) and Soil Canopy Observation, Photochemistry, and Energy Fluxes (SCOPE) models (Wang et al., 2021), the Tethys-Chloris (T&C) model (Fatichi et al., 2012), the Soil-Plant-Atmosphere (SPA) model (Williams et al., 1996; Williams et al., 2001), and the Soil Water Atmosphere Plant (SWAP) model [(van Dam et al., 2008) – specifically the version coupled to the World Food Studies (WOFOST) model (de Wit et al., 2019)]. However, SPAC models either ignore or oversimplify the underlying groundwater system by neglecting spatio-temporal variability in groundwater variables (e.g., head and temperature), and processes (e.g., recharge, discharge and groundwater evapotranspiration). Thus, the SPAC models lack or simplify the groundwater influence on the simulated ~~soil-plant-atmosphere~~SPAC processes.

For most landscapes, groundwater storage is generally the largest component of the local water budget. It plays a vital role in sustaining essential ecosystem services by mitigating biodiversity loss and buffering against climate change (Saccò et al., 2024). Many ecosystems rely primarily on groundwater resources, so-called groundwater-dependent ecosystems, to maintain their ecological functions (Lubczynski, 2009; Kløve et al., 2014). Groundwater-dependent ecosystems can be

exposed to surface water – groundwater interactions, through altered recharge or discharge rates. Such changes may impair their ecological function if groundwater availability declines, particularly under future climate regimes , ~~which enhance groundwater discharge and likely face significant impairment under future climate regimes~~ (Otoo et al., 2025). Groundwater can also have a significant effect ~~in~~ on enhancing carbon assimilation, plant growth and productivity (Ruehr et al., 2023). Under shallow water table conditions, the groundwater dynamics is significant, exerting a strong influence on the soil moisture distribution and the evapotranspiration rates (Martínez-De La Torre & Miguez-Macho, 2019). Additionally, groundwater systems typically respond slower to meteorological forcing, as compared to the surface water or the near-surface soil moisture, due to their larger storage and longer flow paths. This relative hydrological stability allows groundwater to continue supporting vegetation in mitigating water stress effects during prolonged drought periods after soil moisture has been depleted. ~~groundwater processes operate at a slower pace, as compared to surface water systems or the soil zone, leading to latency in their responses to environmental changes, such as drought. This delayed response allows the groundwater to support vegetation in mitigating water stress effects during prolonged drought periods.~~ Marchionni et al. (2020) demonstrated that the presence of the water table within the vegetation rooting depth supported the ecosystem transpiration and vegetation productivity during a prolonged drought event (2001-2009) near Melbourne, Australia.

Groundwater and its interaction with the surface (through the unsaturated zone) are often simulated by integrated hydrological models (IHMs). IHMs simulate flow processes in the surface and subsurface domains, including their dynamic interaction (i.e., flow exchange) within a single simulation environment (Daoud et al., 2022; 2024). ~~IHMs are used for assessing water resources and evaluating future scenarios for sustainable water resources management .~~ Examples of IHMs are Hydrogeosphere (Brunner & Simmons, 2012), MIKE SHE (Graham & Butts, 2005), CATHY (Camporese et al., 2010), and MODFLOW 6 (Langevin et al., 2017; Langevin et al., 2023). However, IHMs do not consider ecosystem functioning, so they do not simulate explicitly the carbon cycle nor detailed

plant processes. Consequently, IHMs are rarely used to evaluate ecosystem functioning and the interactions between the water, energy and carbon cycles, for which SPAC models are used.

Despite the critical role groundwater plays in sustaining many different types of ecosystems, SPAC models, unlike IHMs, typically lack a physically-based groundwater model. Instead, they commonly assume that soil moisture dynamics is primarily driven by infiltration (generated from precipitation or applied irrigation) and either ignore or oversimplify groundwater and its connection to the soil and the vegetation domains (Samuel & Chakraborty, 2023). Notably, SPAC models typically do not account for heterogeneity in any of the aquifer properties, i.e. ~~(~~porous media or fractured-rock systems~~)~~ (Zhang et al., 2020; Agbotui et al., 2025), which can be significant in shaping key groundwater processes such as recharge, capillary rise, and groundwater evapotranspiration (Ireson et al., 2013; Xin et al., 2023). Thus, SPAC models are not equipped to accurately capture the effect of salient groundwater processes while simulating soil and vegetation dynamics. Additionally, SPAC models ignore or simplify spatio-temporal groundwater temperature dynamics. However, many recent studies (Xin et al., 2023; Benz et al., 2024; Egidio et al., 2024; Rammler & Bertermann, 2025) showed that soil temperatures are modulated not only by surface-atmosphere heat exchange processes, but also by soil zone ~~–~~ groundwater heat exchange processes (i.e. conductive and advective heat transport), especially in cases of shallow water table conditions. Ignoring the thermal dynamics of groundwater can subsequently lead to biases in simulating soil temperature, which is a key driver for photosynthesis, evapotranspiration (specifically latent heat flux), and carbon fluxes. Omitting or simplifying the groundwater component (for flow and heat processes) in SPAC models may also lead to misrepresentation of soil and plant physiological responses to changing ambient (climatic) conditions; thereby limiting the usefulness of SPAC models for appraising the impact of a changing climate on groundwater-dependent ecosystems (Elrashidy et al., 2023) or, more generally, ecosystems with shallow groundwater conditions.

Given the limitations of both the SPAC models and IHMs, an integrated modelling approach, that combines hydrology with ecosystem functioning, would result in a modelling tool that is better suited for evaluating ecosystem functioning under a changing climate. An integrated SPAC-IHM model is hereafter referred to as an integrated ecohydrological model (IEM). The advantage of an IEM is that it can simulate the full continuum of water (including groundwater), energy, and carbon fluxes at high spatio-temporal resolution within a single simulation environment. IEMs are also capable of integrating the surface and subsurface hydrology (both unsaturated and saturated zones) with plant physiological processes, as well as incorporating remote-sensing information (as inputs) for simultaneous simulation of multiple variables [i.e., soil moisture (θ), soil temperature (T_s), evapotranspiration (ET), groundwater level (GWL), and groundwater temperature (GT), gross primary productivity (GPP), net ecosystem exchange (NEE), and SIF] that are vital for accurately characterizing ecosystem dynamics. Furthermore, IEMs facilitate the simulation of continuous moisture and temperature profiles from the subsurface to the top of the canopy. Table 1 lists the few existing IEMs that can physically simulate energy, carbon and water processes, including groundwater flow. The list includes the enhanced CLM5 (Akhter et al., 2025), the Terrestrial System Modelling Platform (TerrSysMP, Shrestha et al., 2014; Gasper et al., 2014), the enhanced version (Liao et al., 2025) of the Earth system model (E3SM; Golaz et al., 2022) and the MODFLOW–MetaSWAP–WOFOST (Van Walsum & Supit, 2012). While all these IEMs can simulate the water processes, including detailed groundwater flow processes, they all lack the representation of groundwater heat processes and groundwater temperature simulation. Furthermore, none of them accounts for SIF simulation. Hence, a new IEM is needed that can physically-based integrate the groundwater processes (mass and energy) with detailed energy, carbon and SIF fluxes. The hypothesis of this study is that explicit representation of groundwater mass and energy in an IEM framework would improves quantification of the soil–plant–atmosphere continuum by: a) improving the simulation of soil moisture and temperature profiles; b) enabling two-way feedbacks between the unsaturated and saturated zone and their further impact on water fluxes; and c) revealing the

groundwater's influence on carbon fluxes and vegetation physiological processes such as root water uptake and photosynthesis (reflected by fluorescence). Collectively, testing these hypotheses would unravel the role of groundwater in shaping the SPAC dynamics and ~~and~~ deepen~~s our~~ the understanding of ecosystem functioning.

201 Table 1. List of available integrated ecohydrological models (IEMs)

Model name	Water cycle processes			Heat transfer processes		Energy cycle, ET and root growth & uptake	Carbon cycle and photosynthesis	SIF	Reference
	Surface water (runoff and streamflow)	Unsaturated zone flow	Groundwater flow	Unsaturated zone	Groundwater zone				
Enhanced CLM5	Yes	Yes, 1D Richards equation	Yes, by incorporating an aquifer beneath the soil column to allow for lateral groundwater flow and pumping	Yes	No	Yes	Yes	No	(Akhter et al., 2025)
TerrSysMP (COSMO–CLM3.5–ParFlow)	Yes	Yes, via ParFlow (3D Richards equation)	Yes, via ParFlow (3D Richards equation)	Yes	No	Yes	Yes	No	(Shrestha et al., 2014; Gasper et al., 2014)
Enhanced E3SM	Yes	Yes	Yes, by developing a new hillslope-based hydrological model to simulate lateral groundwater flow	Yes	No	Yes	Yes	No	(Liao et al., 2025)
MODFLOW–MetaSWAP–WOFOST	Yes	Yes, 1D Richards equation	Yes, via MODFLOW (1D/2D/3D).	Yes	No	Yes	Yes, via WOFOST	No	(Van Walsum & Supit, 2012)
STEMMUS–SCOPE–MODFLOW 6	Yes	Yes, 1D Richards equation	Yes, via MODFLOW 6 (1D/2D/3D). 1D is used in this study	Yes	Yes, via MODFLOW 6	Yes	Yes	Yes	This study

202

This study aims to investigate the role of groundwater in the SPAC with a focus on assessing the benefits of explicitly incorporating the groundwater component in modelling SPAC processes. In particular, the specific objectives are to investigate the impacts of the groundwater component (mass and energy) on: 1) regulating the soil profile, in terms of moisture and temperature; 2) the dynamics of the unsaturated/saturated zones and its further impact on water fluxes and root water uptake; and 3) the carbon fluxes and vegetation physiological processes (i.e. root water uptake and photosynthesis reflected by fluorescence). To address these objectives~~this end~~, a new IEM framework is developed by ~~tightly~~ coupling the STEMMUS-SCOPE SPAC model to the MODFLOW 6 IHM model~~. The STEMMUS-SCOPE-MODFLOW 6 is tested in a 1-dimensional (1D) setup (which will be extended to 2D/3D in a follow-up study)~~ and applied at ~~to~~ three sites in the Netherlands (i.e., Loobos, Cabauw, and Veenkampen). Since STEMMUS-SCOPE is a point-based model, ~~while~~ MODFLOW 6 is a grid-based model~~.~~, and ~~As~~ this study is the first example of coupling these two models, the ST-SC-MF6 models were set up in a vertically-stacked orientation (1-dimensional, 1D). The 1D models were assumed to be representative of the ecosystem of each of the corresponding sites. Simulated variables of interest are evaluated with and without the coupling to quantify the effect of explicitly representing groundwater within the simulations.

~~STEMMUS-SCOPE model (Wang et al., 2021) is a SPAC model, which is an integrated version of two separate models (STEMMUS and SCOPE). STEMMUS (Simultaneous Transfer of Energy, Mass, and Momentum in Unsaturated Soil) simulates the transfer of energy, mass, and momentum in the unsaturated zone (Zeng et al., 2011a; b; Zeng & Su, 2013). SCOPE (Soil Canopy Observation, Photochemistry, and Energy Fluxes) simulates the radiative transfer in the soil, leaves, and vegetation canopies, as well as photosynthesis and non-radiative energy dissipation through convection and mechanical turbulence (Van Der Tol et al., 2009; Yang et al., 2021). The coupling between STEMMUS and SCOPE enables the seamless soil-plant-atmosphere modelling of energy, water and carbon exchanges. Additionally, STEMMUS-SCOPE allows for simulating the influence of θ and T_s variability on vegetation dynamics in terms of photosynthesis, stomatal behavior and plant~~

~~water stress responses (Tang et al., 2024). More details about the STEMMUS-SCOPE coupling are described in Wang et al. (2021).~~

~~MODFLOW 6 is an IHM framework (Hughes et al., 2017) and is the latest "core" version of the well-known MODFLOW simulator for groundwater flow (GWF). In addition, MODFLOW 6 simulates other flow and transport processes, including unsaturated zone flow, overland flow, flow in surface features (e.g. lakes, rivers, drains, etc), and their interaction with the groundwater system (Langevin et al., 2017; Langevin et al., 2023). Recently, a new Groundwater Energy Transport (GWE) module, patterned after the solute transport module (Langevin et al., 2022), was added to MODFLOW 6 for simulating heat transport processes within a MODFLOW 6 simulation (Morway et al., 2025) and is leveraged in this study.~~

2. Methods

2.1. Summary of the two coupled models

STEMMUS-SCOPE (~~Y.~~ Wang et al., 2021) is a SPAC model, which is an integrated version of two separate models (STEMMUS and SCOPE). STEMMUS simulates the transfer of energy, mass, and momentum in the unsaturated zone (Zeng et al., 2011a; b; Zeng & Su, 2013). SCOPE simulates the radiative transfer in the soil, leaves, and vegetation canopies, as well as photosynthesis and non-radiative energy dissipation through convection and mechanical turbulence (Van ~~D~~der Tol et al., 2009; Yang et al., 2021). The coupling between STEMMUS and SCOPE enables the seamless SPAC modelling of energy, water and carbon exchanges. Additionally, STEMMUS-SCOPE allows for simulating the influence of θ and T_s variability on vegetation dynamics in terms of photosynthesis, stomatal behavior and plant water stress responses (Tang et al., 2024). More details about the STEMMUS-SCOPE coupling are described in Wang et al. (2021).

MODFLOW 6 is an IHM framework (Hughes et al., 2017) and is the latest "core" version of the well-known MODFLOW simulator of groundwater flow (GWF). In addition, MODFLOW 6 simulates other flow and transport processes, including unsaturated zone flow, overland flow, flow in surface water bodies (e.g. lakes, rivers, drains), and their interaction with the groundwater system (Langevin et al., 2017; Langevin et al., 2023). Recently, a new Groundwater Energy Transport (GWE) module, patterned after the solute transport module (Langevin et al., 2022), was added to MODFLOW 6 for simulating heat transport processes within a MODFLOW 6 simulation (Morway et al., 2025) and it is leveraged in this study.

~~2.1.~~2.2. STEMMUS-SCOPE & MODFLOW 6 coupling

The Basic Model Interface (BMI; Peckham et al., 2013; Hutton et al., 2020) ~~is~~ was adopted as the convention for coupling STEMMUS-SCOPE to MODFLOW 6. The BMI protocol is general; it allows via an external program or script to control models ~~that support it can be controlled,~~ and set their variables ~~can be accessed and set~~ during runtime ~~by an external program or script~~. By ~~BMI protocols are used for this effort to facilitate~~ facilitating the exchange of model-calculated variables and other information between the coupled models ~~by passing values~~ externally~~;~~, the BMI thereby ~~eliminating~~ eliminates the need to access (or modify) the source code(s) of the coupled models during the simulations. That protocol allows for coupling models which are written in different programming languages, as exemplified in this study (STEMMUS-SCOPE in MATLAB and MODFLOW 6 in Fortran). Hence, BMI allows for keeping up with future updates or new versions of the individual models without extensive reconfiguration.

~~2.1.1.~~2.2.1. BMI phases

BMI routines are commonly organized into three phases (initialize, update, finalize) as described in figure 2 of Hughes et al. (2022). Figure 1 shows the coupling framework of STEMMUS-SCOPE-MODFLOW 6.

Initialize phase

The initialization phase in a BMI setup is separate from the initialization routines associated with each of the individual models (explained in Section 2.4.2~~2.4.2~~). During the BMI initialization routine, "hooks" are established between the coupled models to facilitate the exchange of calculated values during a forward run. During the initialize phase, initialized head (i.e., GWL) and temperature (i.e., GT) of the water table are defined in STEMMUS-SCOPE. While, initialized groundwater net recharge flux ($\mathrm{R_n}$), heat flux above water table ($\mathrm{Q_{heat}}$), and net recharge temperature ($\mathrm{RT_n}$) are defined in MODFLOW 6.

Update phase

The update phase is at the core of the coupling process (Fig. 1b). During this phase, the two models exchange variable values at the phreatic surface (the shared interface between the unsaturated zone and the saturated zone, marked by a bold blue line in the diagram of Fig. 1a). At this shared interface, STEMMUS-SCOPE requires the following bottom boundary conditions: a) specified head (i.e. GWL) for the soil water module; and b) specified temperature (i.e. GT) for the soil energy module; together to simulate groundwater gross recharge ($\mathrm{R_g}$), capillary rise flux (Cap), root groundwater uptake ($\mathrm{RWU_g}$), $\mathrm{Q_{heat}}$, and $\mathrm{RT_n}$. In turn, MODFLOW 6 requires the following upper boundary conditions: specified water flux (i.e. $\mathrm{R_n}$, calculated as the difference between $\mathrm{R_g}$, Cap, and $\mathrm{RWU_g}$) for the GWF module, and b) specified heat flux (i.e., $\mathrm{Q_{heat}}$) and/or its specified temperature (i.e., $\mathrm{RT_n}$) for the GWE module; together to simulate GWL and GT. From herein, the simulated variables ($\mathrm{R_n}$, $\mathrm{Q_{heat}}$, and $\mathrm{RT_n}$) by STEMMUS-SCOPE are referred to as 'STEMMUS-SCOPE variables' (marked by red color in the flowchart of Fig. 1b), while the simulated variables by MODFLOW 6 (GWL and GT) are referred to as 'MODFLOW 6 variables' (marked by blue color in the flowchart of Fig. 1b).

The update phase runs in a looped manner (update loop) with number of updates equal to number of time steps. In principle, the BMI can work with different temporal discretization (number of time steps and the length of each time step) for each of the two coupled models. However, for ease of

use, the same temporal discretization was used for both models in this study. For each time step: 1) MODFLOW 6 runs and updates the MODFLOW 6 variables; 2) the updated MODFLOW 6 variables are passed to STEMMUS-SCOPE (illustrated by the blue bold arrow in Fig. 1b), which are used as bottom boundary conditions by STEMMUS-SCOPE; 3) STEMMUS-SCOPE runs and updates the STEMMUS-SCOPE variables; 4) the updated STEMMUS-SCOPE variables are passed back to MODFLOW 6 (illustrated by the red bold arrow in Fig. 1b) to be used as upper boundary conditions for the next time step; and 5) updates continue until the last time step.

Finalize phase

In this phase, both models finalize their simulation, and the model outputs are exported for further analysis. The model outputs include the STEMMUS-SCOPE variables, the MODFLOW 6 variables, and other variables of interest (marked by black color in Fig. 1) as follows: θ, T_s, root soil water uptake (RWU_s), subsurface evaporation (E_{ss}), ET which is the summation of E_{ss}, RWU_s and RWU_g, GPP, NEE, and SIF.

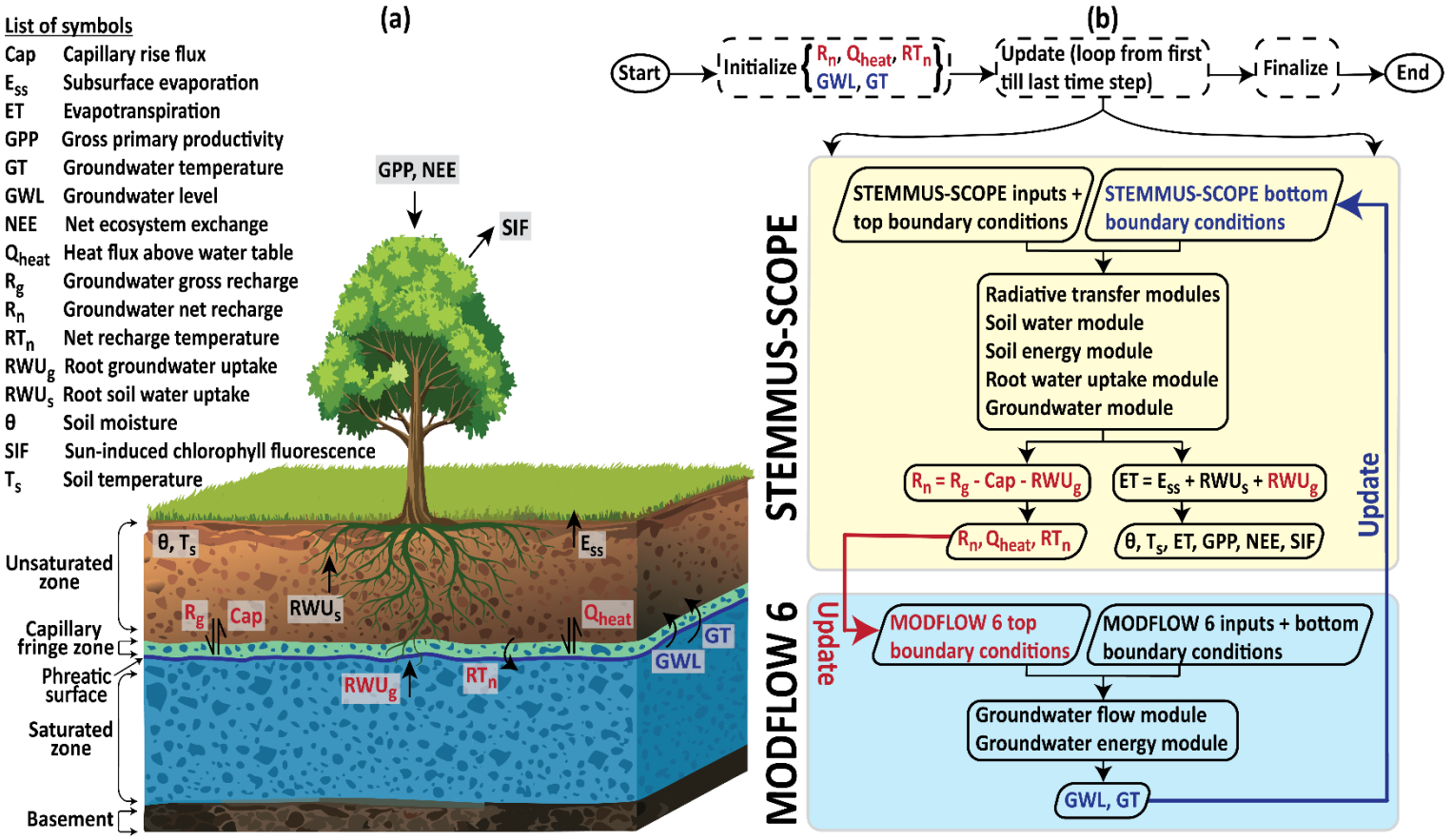


Figure 1. Schematic of the coupled STEMMUS-SCOPE and MODFLOW 6 framework: a) illustrative diagram (left panel); b) flowchart (right panel). The red color indicates the processes and/or variables that are transferred from STEMMUS-SCOPE to MODFLOW 6. The blue color indicates the processes and/or variables that are transferred from MODFLOW 6 to STEMMUS-SCOPE.

MODFLOW 6 was not originally written to support BMI; however, Hughes et al. (2022) documents the restructuring of the source code to align MODFLOW 6 to support the BMI conventions. Similarly, Schilperoort (2025) and Zeng et al. (2025) document the steps followed to make STEMMUS-SCOPE BMI-compatible. Additionally, a groundwater module is added into the source code of STEMMUS-SCOPE to: a) recognize the effect of the saturated zone dynamics on the unsaturated zone through the MODFLOW 6 variables; and b) prepare the necessary STEMMUS-SCOPE variables that are fed into MODFLOW 6. The groundwater module includes three main parts: 1) unsaturated zone bottom boundary; 2) recharge and capillary rise flux; and 3) root groundwater uptake.

~~2.1.2.~~2.2.2. Unsaturated zone bottom boundary

The bottom boundary of the unsaturated zone for the soil water module in STEMMUS-SCOPE can be defined using one of three options (Zeng & Su, 2013): a) specified matric head (Dirichlet) boundary; b) specified moisture flux; and c) zero matric head (i.e. gravity drainage). For this investigation, option (a) is used. This bottom boundary (specified matric head) is adaptively positioned at the phreatic surface (Fig. 1a), corresponding to the GWL at each time step (Zeng et al., 2019). The GWL value is received by STEMMUS-SCOPE from MODFLOW 6 through the BMI (Fig. 1b). Then, at the phreatic surface elevation (GWL), the specified matric head is set to zero (matric head is negative above GWL and positive below GWL). At each time step, the GWL may rise or fall, causing the phreatic surface to shift upward or downward. As a result, the thickness of the unsaturated zone decreases or increases, and the position of the bottom boundary is updated to reflect this moving boundary condition.

Similarly, for the soil energy module, a specified temperature boundary condition is used as the bottom boundary. The value of the specified temperature is the GT (Fig. 1b), received by STEMMUS-SCOPE from MODFLOW 6 through the BMI and updated at each time step.

~~2.1.3.~~2.2.3. Recharge and capillary rise flux

STEMMUS-SCOPE simulates two-phase mass and heat flow in the unsaturated zone using the modified Richards equation (Milly, 1982). The water flow is driven by both gravity and capillary forces (Eq. 1).

$$\frac{\delta}{\delta t}(\rho_L\theta_L + \rho_v\theta_v) = \frac{-\delta}{\delta z}(q_{Lh} + q_{LT} + q_{vh} + q_{vT}) - S$$

$$= \rho_L \frac{\delta}{\delta z}\left[K\left(\frac{\delta\psi}{\delta z} + 1\right) + D_{Ta}\frac{\delta T}{\delta z}\right] + \frac{\delta}{\delta z}\left[D_{vh}\frac{\delta\psi}{\delta z} + D_{vT}\frac{\delta T}{\delta z}\right] - S \quad (1)$$

where ρ_L and ρ_v (kg m^{-3}) are the density of liquid water and water vapor, respectively; θ_L and θ_v (m^3 m^{-3}) are the soil liquid and vapor volumetric water content, respectively; q_{Lh} and q_{LT} (kg m^{-2} s^{-1}) are the soil liquid water fluxes driven by the soil matric potential gradient ($\frac{\delta\psi}{\delta z}$) and temperature gradient ($\frac{\delta T}{\delta z}$), respectively; q_{vh} and q_{vT} (kg m^{-2} s^{-1}) are the soil water vapor fluxes driven by the $\frac{\delta\psi}{\delta z}$ gradient and the $\frac{\delta T}{\delta z}$ gradient, respectively; K is the unsaturated hydraulic conductivity (m s^{-1}); D_{Ta} (m^{-2} s^{-1} K^{-1}) is the transport coefficient of the adsorbed liquid flow due to temperature gradient; D_{vh} (kg m^{-2} s^{-1}) is the isothermal vapor conductivity; D_{vT} (kg m^{-1} s^{-1} K^{-1}) is the thermal vapor diffusion coefficient, and S is the sink term (m s^{-1}). More details of the equation are in Zeng et al. (2011a, b) and Zeng & Su (2013).

As explained in Section ~~2.1.1~~ 2.2.1, the GWL is adopted as the bottom boundary condition of the unsaturated zone in STEMMUS-SCOPE. Consequently, a capillary fringe zone is formed above the phreatic surface (Fig. 1a), where water is pulled up from the saturated zone by capillary forces. Moreover, when precipitation infiltrates into the unsaturated zone and percolates downward, it has to go through the capillary fringe zone and continue downward as R_g to the saturated zone. Hence, the capillary fringe zone includes both the R_g and the Cap. The R_g and the capillary rise flux (Cap), the latter contributes to groundwater evaporation (Balugani et al., 2017), are calculated from the summation of q_{Lh}, q_{LT}, q_{vh}, and q_{vT} fluxes (Eq. 2) at the capillary fringe zone. The result of that

summation determines whether the calculated flux (Q, Eq. 2a) represents R_g or Cap. If the summation is negative (Eq. 2b), it means the flow direction is downward, and the R_g term is dominant. In contrast, if the summation is positive (Eq. 2c), it means the flow direction is upward, and the Cap term is dominant. In STEMMUS-SCOPE, upward fluxes (capillary rise) are positive, while downward fluxes (gravity drainage) are negative. However, MODFLOW 6 uses the opposite sign convention. Therefore, the R_g/Cap is multiplied by -1, when transferred to MODFLOW 6 through the BMI.

$$Q = q_{Lh} + q_{LT} + q_{vh} + q_{vT} \quad (2a)$$

$$R_g = Q \quad \text{if } Q < 0 \quad (2b)$$

$$Cap = Q \quad \text{if } Q \geq 0 \quad (2c)$$

~~2.1.4.~~2.2.4. Root groundwater uptake

The root water uptake (RWU) is calculated in STEMMUS-SCOPE based on a resistance scheme that takes into account the hydraulic gradient between the soil water potential (ψ_i) and the leaf water potential (ψ_l) (Eq. 3). The root water uptake module, developed by Wang et al. (2021), takes into account the θ as the only source of water for the roots (root soil water uptake, RWU_s), meaning that RWU = RWU_s. The RWU_s is calculated for all the soil layers that are above the maximum rooting depth (d_{max}).

$$RWU = \sum_{i=1}^{n} \frac{\psi_{s,i} - \psi_l}{r_{s,i} + r_{r,i} + r_{x,i}} \text{ and } RWU_s = RWU \quad (3)$$

where $\psi_{s,i}$ is the soil water potential of layer i (m), ψ_l is leaf water potential (m), $r_{s,i}$ is the soil hydraulic resistance (s m^{-1}), $r_{r,i}$ is the root resistance to water flow radially across the roots (s m^{-1}), and $r_{x,i}$ is the plant's axial resistance to flow from the root xylem to the leaves (s m^{-1}).

However, the roots can uptake water from an additional source (root groundwater uptake, RWU_g) if the roots have access to groundwater (GWL is above d_{max}). As explained in Section ~~2.1.1~~2.2.1, the

GWL is adopted as the bottom boundary condition of the unsaturated zone for the soil water module in STEMMUS-SCOPE, hence, the RWU can also be influenced. The RWU calculations were updated by splitting it into two components (RWU_s and RWU_g, Eq. 4). The RWU_s is for the soil layers that are above the capillary fringe and above d_{max} (Eq. 5), and the RWU_g is for the soil layers that are below the capillary fringe zone and above d_{max} (Eq. 6). The RWU_s and RWU_g are calculated by replacing the soil water potential ($\psi_{s,i}$) in Equation 4 with the updated $\psi_{s,i}$ (due to the effect of GWL) in Equation 5), and with the groundwater potential ($\psi_{g,i}$) in Equation 6, respectively.

$$RWU = RWU_s + RWU_g \quad (4)$$

$$RWU_s = \sum_{i=1}^{n} \frac{\psi_{s,i} - \psi_l}{r_{s,i} + r_{r,i} + r_{x,i}} \text{ for the soil layers above capillary fringe zone and above } d_{max} \quad (5)$$

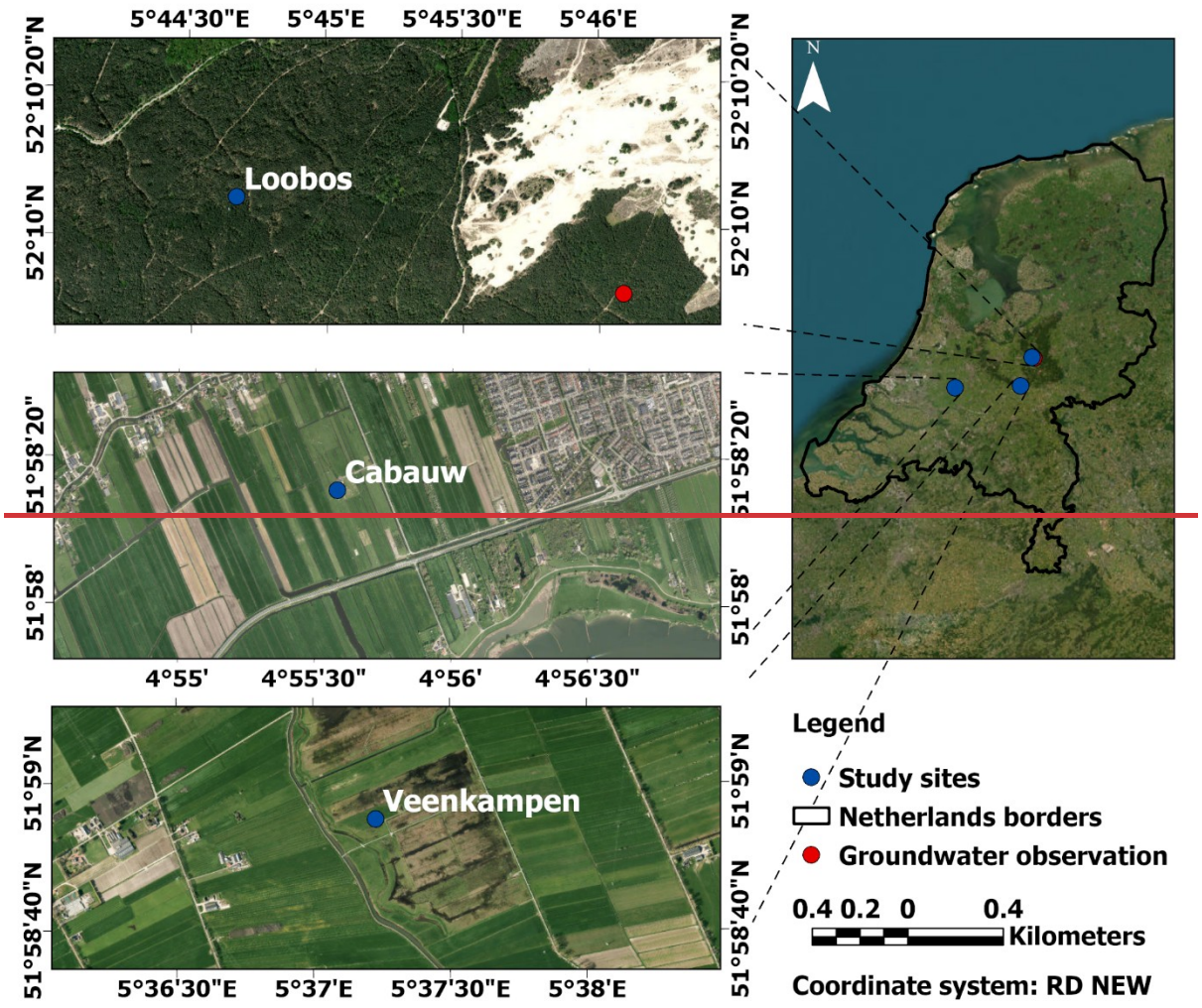
$$RWU_g = \sum_{i=1}^{n} \frac{\psi_{g,i} - \psi_l}{r_{s,i} + r_{r,i} + r_{x,i}} \text{ for the soil layers below capillary fringe zone and above } d_{max} \quad (6)$$

For soil layers below d_{max}, RWU = RWU_g = 0

~~2.2.~~2.3. Study sites and data

The proposed model coupling was applied to ~~3~~ three sites in the Netherlands covering both forest (Loobos) and meadow (Cabauw and VeenKampen) ecosystems (Fig. 2). Those three sites were selected because: a) they provide comprehensive in-situ measurements spanning the water, energy, and carbon cycles, including meteorological forcing, different observations such as θ and T_s profiles, eddy covariance flux measurements (e.g. ET, GPP, and NEE), groundwater variables (i.e. GWL and GT), and vegetation characteristics (e.g. SIF) — such data density is essential for rigorously testing the hypothesis of this study and evaluating the developed coupled modelling framework; and b) the sites represent two dominant Dutch landscapes (forest on sandy soil; meadow on clay/peat), allowing preliminary assessment of model transferability across ecosystem types. The ~~3~~ three sites have the typical temperate climate of the Netherlands, with an annual average precipitation of 700-900 mm yr^{-1} (Buishand et al., 2010; Brakkee et al., 2022), and air temperature of 10.5 °C (Bense &

Kurylyk, 2017; Jansen et al., 2023). The Loobos site is located in the forested area of the Veluwe in the central part of the Netherlands, with an elevation of 25.0 m above sea level (a.s.l.) (Table 2). The land cover is evergreen coniferous forest, and the soil type is loamy sandy soil (Heinen et al., 2021). The groundwater depth ranges from 3 to 5 m below land surface (van der Molen et al., 2024; Zhao et al., 2026). The Cabauw site is located in the central western region of the Netherlands, with an elevation of -0.7 m a.s.l.~~below sea level~~ (Table 2). The land cover is grass, and the soil is a mixture of clay and peat (Heinen et al., 2021). The groundwater depth ranges from 0~~.0~~ to 1.25 m below land surface. The Veenkampen site is located in the Veluwe area in the central part of the Netherlands, with an elevation of 5.6 m a.s.l. (Table 2). The land cover is grass, and the soil is thin peat underlain by a clayey sand (Heinen et al., 2021). The groundwater depth ranges from 0.25 to 1 m below land surface.



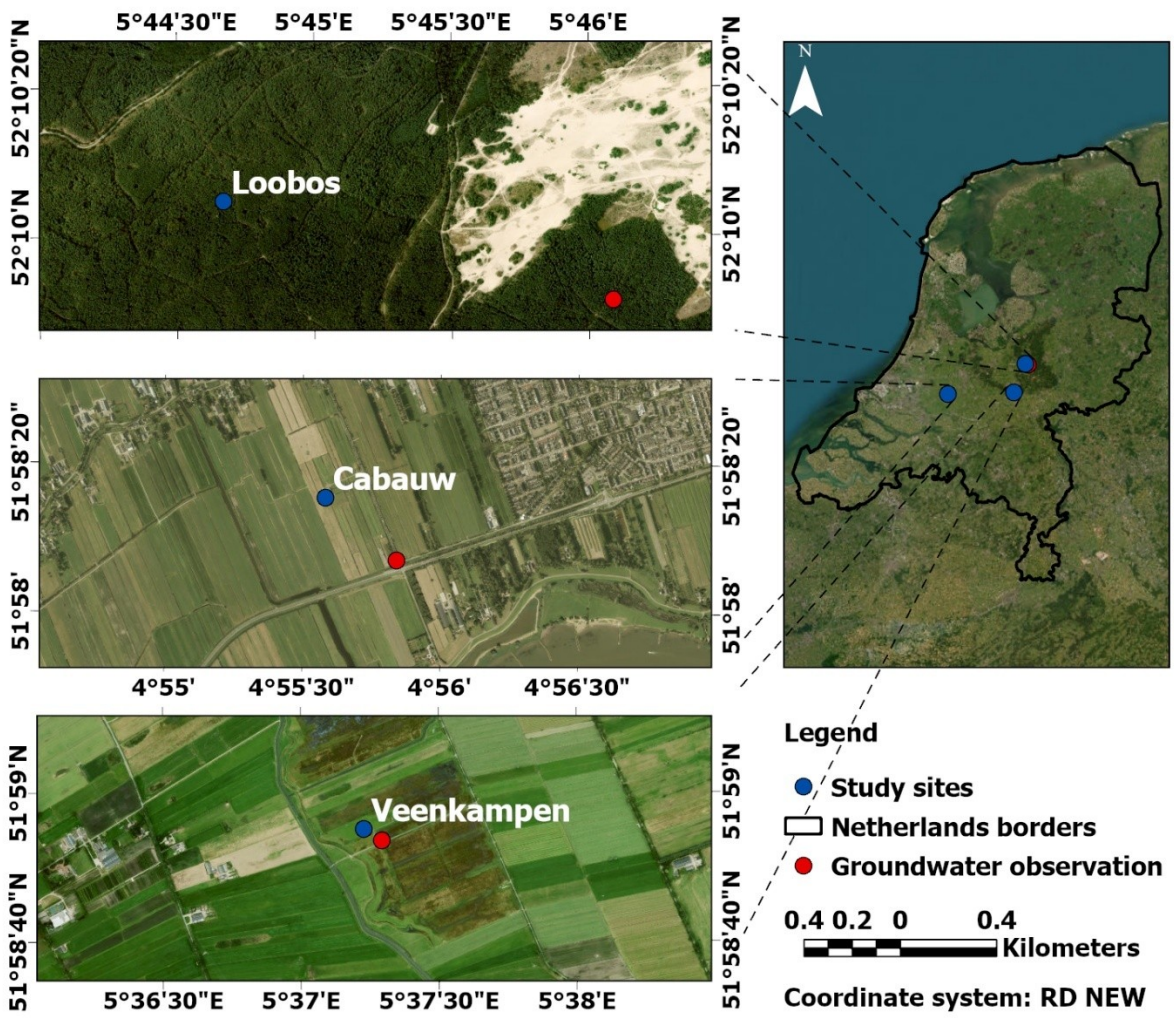


Figure 2. Location of the ~~3~~ three study sites. Images are generated for the day 20 March 2025 using the ESRI ArcGIS Pro software

Table 2. Summary of site characteristics and model discretization

Feature	Loobos	Cabauw	Veenkampen
Elevation (m a.s.l.)	25.0	-0.7	5.6
Land cover	Evergreen coniferous forest	Meadow (grass)	Meadow (grass)
Soil type	Loamy sand	Mix of peat and clay	Mix of peat and clay
Groundwater depth (m) below land surface level	3.0 – 5.0	0.0 – 1.25	0.25 – 1.0

Unsaturated zone discretization:			
Thickness (m)	5.0	1.5	1.2
Number of vertical layers in STEMMUS-SCOPE	69	50	33
Layers thickness range (cm)	1 – 20	1 – 20	1 – 20
Saturated zone discretization:			
Thickness (m), limited to upper-most permeable hydrological unit	20	9	9
Number of vertical layers in MODFLOW 6	20	15	18
Layers thickness range (m)	0.25 – 1.0	0.25 – 1.0	0.25 – 1.0

The forcing inputs and observations data for the ~~3~~ three sites were collected from different sources (Table 3~~Table 2~~). The Meteorology and Air Quality (MAQ) dataset is an open-access collection of harmonized meteorological variables, eddy covariance fluxes, and soil observations for the Loobos and Veenkampen sites, maintained by Wageningen University (van der Molen et al., 2024; Heusinkveld et al., 2024; Zhao et al., 2026). Similarly, the Cesar dataset, operated by the Royal Netherlands Meteorological Institute (KNMI), provides a wide suite of measurements including remote sensing, eddy covariance, surface, soil and hydrological measurements in the Cabauw site (Bosveld, 2020; KNMI, 2024). The forcing inputs include time series of the meteorological inputs (i.e., precipitation, net radiation, air temperature, wind speed, relative humidity, atmospheric pressure, and CO_2 dioxide concentration) and the leaf area index (LAI). For Loobos and Veenkampen, the meteorological inputs and observation datasets were retrieved from the MAQ dataset, while those for the Cabauw site were retrieved from the Cesar dataset (Table 3). The LAI for the three sites was retrieved from the remote sensing MODIS product (MCD15A3H v061, Myneni et al., 2021). The observation datasets include time series of θ, T_s, ET, GPP, NEE, GWL, GT, and SIF. Among all observations, θ and T_s profiles, as well as ET, were available for most of the simulation period, except for short gaps, at the three sites. The ET observations were derived from eddy covariance

Formatte
Italic

Formatte
Italic

towers at the three sites, representing actual ET. GPP was available only at the Loobos site for the period 2016-2021, while NEE was available only at the Cabauw site for the period 2016-2020. GWL was available at Cabauw and Veenkampen from observation wells located close to the main measurement infrastructure (i.e. eddy covariance tower) (Fig. 2). While at Loobos, GWL was not available exactly within the site, but obtained from the nearest available observation point (approximately 500 m away; Fig. 2) via the Data and Information of the Dutch Subsurface (DINOloket) dataset (GDN, 2024). GT was available only at the Loobos site for only one year (1 April 2023 – 31 March 2024). SIF observations were available only at Cabauw on certain days in 2022 and 2023 and were collected by Colombo et al. (2024). All the collected datasets were processed and formatted to be compatible with the needed formats (NetCDF for STEMMUS-SCOPE and ASCII for MODFLOW 6). ~~The observation datasets, available for the entire simulation period, except for short gaps, at the 3 sites, were the profiles of θ and T_s, and ET. Other observation datasets were incomplete and include: a) the GPP, available only at the Loobos site for the period 2016-2021; b) the NEE, available only at the Cabauw site for the period 2016-2020; c) the GWL, not available exactly in the Loobos site, but retrieved from the nearest observation point about 500 m away (the red circle point in Fig. 2), assuming the same GWL; d) the GT, available only at the Loobos site for only one year (from 1 April 2023 to 31 March 2024); and e) the SIF data, available only at the Cabauw site on certain days in 2022 and 2023.~~

Table 3. Datasets acquisition at the ~~3~~ three sites

Data	Loobos	Cabauw	Veenkampen
Meteorological inputs (precipitation, net radiation, air temperature, wind speed, relative humidity, atmospheric pressure and CO_2 dioxide concentration)	MAQ dataset (van der Molen et al., 2024; Zhao et al., 2026)	Cesar dataset (Bosveld, 2020; KNMI, 2024)	MAQ dataset (Heusinkveld et al., 2024)

Leaf area index	MODIS-LAI (Myneni et al., 2021)		
Observations (in-situ measurements)			
Evapotranspiration, soil moisture, soil temperature	MAQ dataset	Cesar dataset	MAQ dataset
Groundwater level	DINOloket (GDN, 2024)	Cesar dataset	MAQ dataset
Groundwater temperature	MAQ dataset	Not available	Not available
Carbon fluxes (gross primary productivity and/or net ecosystem exchange)	MAQ dataset	Cesar dataset	Not available
Sun-induced chlorophyll fluorescence	Not available	(Colombo et al., 2024)	Not available

~~2.3.~~2.4. Models' setup

For brevity, from herein, the STEMMUS-SCOPE model is referred to as ST-SC and the STEMMUS-SCOPE-MODFLOW 6 model is referred to as ST-SC-MF6.

~~2.3.1.~~2.4.1. Temporal and spatial discretization

Both ST-SC and ST-SC-MF6 models of the ~~3~~ three sites used a ~~3~~ three month~~s~~ model initialization phase (i.e. "spin-up") that extended from 1 January 2016 to 31 March 2016. After this, the simulation was run for a period of 8 years (1 April 2016 – 31 March 2024). The total simulation had 144,624 half-hourly time steps.

~~STEMMUS-SCOPE is a point-based model, while MODFLOW 6 is a grid-based model. As this study is the first example of coupling these two models, the ST-SC-MF6 models were set up in a vertically-stacked orientation (1-dimensional, 1D). The 1D models were assumed to be representative of the ecosystem of each of the corresponding sites.~~

The unsaturated zone in STEMMUS-SCOPE was modelled with site-specific total thicknesses: 5 m for Loobos, 1.5 m for Cabauw, and 1.2 m for Veenkampen – each equals to or exceeds the site's maximum observed water table depth (5.0 m for Loobos, 1.25 m for Cabauw, and 1.0 m for

519 Veenkampen). The unsaturated zone was vertically discretized into 69, 50, and 33 layers for Loobos,
520 Cabauw, and Veenkampen, respectively (Table 2). The thickness of the layers was variable (minimum
521 of 1 cm and maximum of 20 cm), started with fine~~r~~ resolution near the surface (1 cm), gradually
522 increased to 20 cm, then gradually decreased again to 5 cm near the water table fluctuation zone.

523 The MODFLOW 6 models were horizontally discretized into a single cell that is 1 m by 1 m, and were
524 vertically discretized into 20, 15, and 18 layers for the Loobos, Cabauw and Veenkampen sites,
525 respectively (Table 2). The layering information was retrieved from the BRO GeoTOP v1.6. geological
526 model (TNO – GDN, 2023) and the BRO REGIS II v2.2.2. hydrogeological model (TNO – GDN, 2024).
527 Since the models were 1D models in the vertical direction, lateral flow considerations were
528 neglected. To minimize the effect of this negligence, the saturated zone simulation was limited to
529 the upper-most permeable hydrogeological unit, which terminates at a depth of 20 m below the
530 land surface for Loobos and 9 m for both the Cabauw and Veenkampen sites. This permeable
531 hydrogeological unit was then sub-divided into thinner layers, started with a thickness of 0.25 m,
532 then smoothly increased to 0.5, 0.75, and 1 m. At the base of the bottom-most active layer, a
533 specified flux boundary condition was applied to compensate for the vertical flow of the excluded
534 deeper hydrogeological units.

535 ~~2.3.2.~~2.4.2. Initial and boundary conditions

536 Each model of the ~~3~~ three sites was initialized by an initial θ and T_s for STEMMUS-SCOPE, and an
537 initial GWL and GT for MODFLOW 6. The initial θ, T_s, GWL, and GT values were retrieved from the
538 collected datasets (Table 3~~Table 2~~) of the ~~3~~ three sites as follows: a) 0.1, 5°C, 21.5 m, and 10°C for
539 Loobos, b) 0.6, 5°C, -0.8 m and 10.5°C for Cabauw, and c) 0.75, 5°C, 5.1 m, and 11°C for
540 Veenkampen.

Formatte
Italic

541 The top boundary of the soil water module in STEMMUS-SCOPE was a specified flux (precipitation,
542 input retrieved from the collected datasets in Table 3~~Table 2~~), and the bottom boundary was the
543 GWL (received from MODFLOW 6). The top boundary of the soil energy module in STEMMUS-SCOPE

Formatte
Italic

was a specified temperature (air temperature, input retrieved from the collected datasets in Table 3~~Table 2~~), and the bottom boundary was the GT (received from MODFLOW 6). The top boundary of the GWF module of the saturated zone in MODFLOW 6 was the R_n (received from STEMMUS-SCOPE), and the bottom boundary was a specified flux (unknown value that was initially set to 0.0005 m day^{-1} and calibrated later). The top boundary of the GWE module of the saturated zone in MODFLOW 6 was the Q_{heat} and RT_n (received from STEMMUS-SCOPE), and the bottom boundary was a specified heat flux (unknown value that was initially set to 0.05 W m^{-2} and calibrated later).

~~2.3.3.~~2.4.3. Model parameters and calibration/validation

Both STEMMUS-SCOPE and MODFLOW 6 models have ~~a lot of~~several parameters – herein, only the parameters that had a high impact on the simulations (based on an earlier sensitivity analysis) are calibrated and listed in Table 4. The main parameters that govern the flow simulation in STEMMUS-SCOPE were: the vertical saturated hydraulic conductivity of the unsaturated zone (K_{sat}), residual water content (θ_r), saturated water content (θ_s), empirical coefficients of the Van Genuchten equation (α and n), and d_{max}. In MODFLOW 6, the main aquifer parameters were: the horizontal (K_h) and vertical (K_v) hydraulic conductivity, specific storage (S_s), and specific yield (S_y). Both STEMMUS-SCOPE and MODFLOW 6 used the same thermal parameters to simulate the heat transfer in both the unsaturated and the saturated zones, including: thermal conductivity of solids (K_T), specific heat capacity of solids (c_s), and bulk density (ρ_s). ~~All the parameters in Table 4 were initialized with default values (not presented) and further calibrated.~~ As explained in Section 2.4.1, the soil profiles at each site were discretized into multiple vertical layers (Table 2) to account for soil heterogeneity. Initially, all layers were assigned uniform values for each parameter. During the calibration procedure, these parameters were updated individually for each layer to reflect the vertical variability of the θ and T_s measurements. The ranges of the calibrated values for each parameter across the layers are summarized in Table 4.

Formatte
Italic

Formatte
Italic, Che

The 8-year simulation period was divided into a 4-year calibration period (1 April 2016 – 31 March 2020), followed by a 4-year validation period (1 April 2020 – 31 March 2024). The collected observation datasets (Table 3~~Table 3~~) were used as calibration/validation state variables for the calibration/validation periods, respectively. The models were calibrated by trial and error until ~~a~~ satisfactory qualitative (graphical) and quantitative (statistical) matches between the simulated variables and their observed equivalents were achieved. The goodness of fit was assessed using two statistical metrics: the Kling–Gupta efficiency (KGE; Gupta et al., 2009) and the root mean square error (RMSE). The KGE value can range from negative infinity to 1 and was deemed acceptable, when it was larger than zero (Knoben et al., 2019). The RMSE value was deemed acceptable, when it was minimized to 0.1 $m^3\ m^{-3}$, 2°C, 0.5 m, 1°C, 1 mm day^{-1}, 3 gC $m^{-2}\ day^{-1}$, 5 gC $m^{-2}\ day^{-1}$, and 0.25 mW m^{-2} $\mu m^{-1}\ sr^{-1}$ for θ, T_s, GWL, GT, ET, GPP, NEE, and SIF, respectively, as similar ranges were indicated in former studies (Lekula & Lubczynski, 2019; Pacheco-Labrador et al., 2019; Thum et al., 2019; Van der Velde et al., 2023; Benz et al., 2024; Qian et al., 2024; Yang & Lei, 2024; Wang et al., 2026).

Table 4 Models' tuned parameters

Parameter		Loobos	Cabauw	Veenkampen	Unit	Model
		Calibrated values				
K_{sat}	Vertical saturated hydraulic conductivity	2.5-10	10-20	10-20	cm day^{-1}	STEMMUS-SCOPE
θ_r	Residual water content	0.03	0.2	0.15	$m^3\ m^{-3}$	STEMMUS-SCOPE
θ_s	Saturated water content	0.2-0.4	0.60-0.62	0.72-0.77	$m^3\ m^{-3}$	STEMMUS-SCOPE
α	Alpha coefficient of Van Genuchten equation	0.1	0.05-0.09	0.02-0.04	cm^{-1}	STEMMUS-SCOPE
n	n coefficient of Van Genuchten equation	3.0-5.0	1.2-2.4	1.8-2.4	-	STEMMUS-SCOPE
d_{max}	Maximum rooting depth	4~~00~~	0.5~~0~~	0.5~~0~~	~~c~~m	STEMMUS-SCOPE
K_h	Horizontal hydraulic conductivity	5.0	5.0	5.0	m day^{-1}	MODFLOW 6
K_v	Vertical hydraulic conductivity	5.0	5.0	5.0	m day^{-1}	MODFLOW 6
S_s	Specific storage	10^{-5}	$1.5*10^{-5}$	$1.5*10^{-5}$	-	MODFLOW 6

S_y	Specific yield	0.05	0.15	0.15	m^{-1}	MODFLOW 6
K_T	Thermal conductivity of solids	1.0-3.0	0.5-1.0	0.5-1.0	W m^{-1} °C^{-1}	Both models
c_s	Specific heat capacity of solids	800-3000	2500-4000	2500-4000	J kg^{-1} °C^{-1}	Both models
ρ_s	Bulk density of solids	900-1600	1200-1600	1200-1600	kg m^{-3}	Both models

3. Results

3.1. Overall models' performance

The θ simulation of the ST-SC-MF6 demonstrated better agreement with the observations during both the calibration and validation periods as compared to the ST-SC simulations at the three sites. The depth-averaged KGE values of θ were increased by 0.29 at Loobos, 0.30 at Cabauw, and 0.21 at Veenkampen (Table 5), while the depth-averaged RMSE values were decreased by 0.02, 0.18, 0.13 at Loobos, Cabauw and Veenkampen, respectively (Table 6).

The T_s improvement of the ST-SC-MF6 simulations were site-dependent. The depth-averaged KGE values of T_s were increased by 0.19 and 0.14 at Loobos and Cabauw, respectively, while increasing slightly in Veenkampen by 0.04 (Table 5). Corresponding RMSE reductions were 0.9, 0.7, 0.2 °C at Loobos, Cabauw and Veenkampen, respectively (Table 6).

The ET improvement of the ST-SC-MF6 simulations were consistent across the three sites, with KGE increases of 0.35, 0.11, 0.15, accompanied by RMSE reductions of 0.38, 0.19, 0.25 mm day^{-1} at Loobos, Cabauw and Veenkampen (Tables 5 and 6), respectively.

The carbon flux responses were site-dependent. At Cabauw, the KGE of NEE increased by 0.18, and the RMSE decreased by 2.4 gC m^{-2} day^{-1} (Tables 5 and 6). While in Loobos, the GPP showed negligible changes between the ST-SC and ST-ST-MF6 simulations, i.e. changes in KGE and RMSE values were limited to 0.1, and 0.1 gC m^{-2} day^{-1}, respectively (Tables 5 and 6).

For SIF at Cabauw, improvement of the ST-SC-MF6 simulation were satisfactory, with KGE increases of 0.15 and RMSE reduction of 0.17 mW m^{-2} μm^{-1} sr^{-1}, respectively (Tables 5 and 6).

Considering the groundwater variables (GWL and GT) in the ST-SC-MF6 simulation, the KGE values for GWL were 0.46 at Loobos, 0.63 at Cabauw, and 0.47 at Veenkampen, and RMSE values of 0.49, 0.21, and 0.26 m, respectively. For GT at Loobos, the KGE value was 0.56 with corresponding RMSE of 0.47 °C.

Table 5. KGE values of the calibration state variables for the STEMMUS-SCOPE (ST-SC) and STEMMUS-SCOPE-MODFLOW 6 (ST-SC-MF6) models at the three sites over the entire period simulation

Variable	Loobos				Cabauw				Veenkampen			
		ST-SC	ST-SC-MF6	Difference (Δ)		ST-SC	ST-SC-MF6	Δ		ST-SC	ST-SC-MF6	Δ
Θ at	20 cm	0.02	0.29		20 cm	0.29	0.71		7 cm	0.49	0.53	
depth	50 cm	0.01	0.46		35 cm	0.37	0.67		13 cm	0.42	0.72	
	100 cm	0.02	0.18		55 cm	0.49	0.65		25 cm	0.46	0.71	
	Average	0.02	0.31	+0.29	Average	0.38	0.68	+0.30	Average	0.45	0.66	+0.21
T_s at	20 cm	0.42	0.49		20 cm	0.65	0.84		10 cm	0.72	0.86	
depth	50 cm	0.33	0.49		35 cm	0.67	0.77		20 cm	0.83	0.84	
	100 cm	0.22	0.56		55 cm	0.64	0.78		50 cm	0.77	0.73	
	Average	0.32	0.51	+0.19	Average	0.65	0.79	+0.14	Average	0.77	0.81	+0.04
GWL		-	0.46	-		-	0.63	-		-	0.47	-
GT		-	0.56	-		-	-	-		-	-	-
ET		0.11	0.46	+0.35		0.65	0.76	+0.11		0.46	0.61	+0.15
GPP		0.47	0.46	-0.01		-	-	-		-	-	-
NEE		-	-	-		0.01	0.19	+0.18		-	-	-
SIF		-	-	-		0.31	0.46	+0.15		-	-	-

Table 6. RMSE values of the calibration state variables for the STEMMUS-SCOPE (ST-SC) and STEMMUS-SCOPE-MODFLOW 6 (ST-SC-MF6) models at the three sites over the entire period simulation

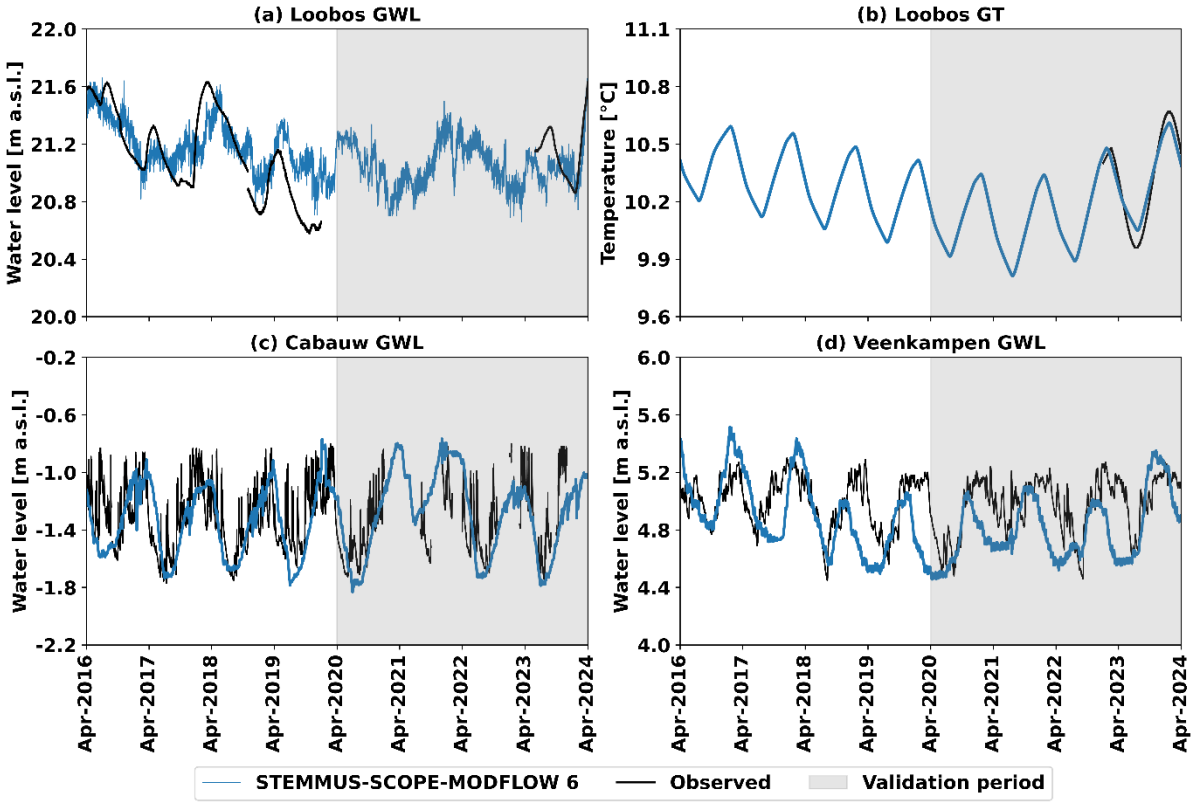
Variable	Unit		Loobos				Cabauw				Veenkampen		
			ST-SC	ST-SC-MF6	Difference (Δ)		ST-SC	ST-SC-MF6	Δ		ST-SC	ST-SC-MF6	Δ
θ at depth	$m^3\ m^{-3}$	20 cm	0.05	0.03		20 cm	0.24	0.08		7 cm	0.24	0.12	
		50 cm	0.04	0.02		35 cm	0.27	0.1		13 cm	0.19	0.08	
		100 cm	0.04	0.02		55 cm	0.28	0.08		25 cm	0.25	0.09	
		Average	0.04	0.02	-0.02	Average	0.26	0.08	-0.18	Average	0.22	0.09	-0.13
T_s at depth	°C	20 cm	2.4	1.7		20 cm	1.8	1.1		10 cm	2.5	2.1	
		50 cm	2.4	1.4		35 cm	1.9	1.2		20 cm	2.2	2.2	
		100 cm	2.7	1.7		55 cm	1.7	1.1		50 cm	2.9	2.5	
		Average	2.5	1.6	-0.9	Average	1.8	1.1	-0.7	Average	2.5	2.3	-0.2
GWL	m		-	0.49	--		-	0.21	--		-	0.26	--
GT	°C		-	0.47	--		-	-	--		-	-	--
ET	$mm\ day^{-1}$		1.37	0.99	-0.38		0.95	0.76	-0.19		1.12	0.87	-0.25
GPP	$gC\ m^{-2}\ day^{-1}$		2.7	2.8	+0.1		-	-	-		-	-	-
NEE	$gC\ m^{-2}\ day^{-1}$		-	-	-		7.0	4.6	-2.4		-	-	-
SIF	$mW\ m^{-2}\ \mu m^{-1}\ sr^{-1}$		-	-	-		0.38	0.21	-0.17		-	-	-

3.2. Saturated zone dynamics

The coupled ST-SC-MF6 model reproduced GWL and GT dynamics with overall satisfactory KGE and RMSE performance across the three sites (Section 3.1). At the three sites, the ST-SC-MF6 models successfully captured the observed GWL rise during wet periods and drawdown during dry periods (Figure 3). At Cabauw and Veenkampen, the shallow water table exhibited pronounced groundwater – soil coupling, which directly influenced root-zone moisture and propagated upward to ecosystem fluxes. In contrast, at Loobos, the relatively moderate groundwater depths and poor soil

characteristics resulted in weak hydraulic connectivity with the unsaturated zone, limiting its influence on upper soil layers moisture dynamics. However, the ST-SC-MF6 model successfully reproduced the seasonal GT variability (Figure 3) with satisfactory KGE and RMSE performances, demonstrating the ability of the coupled model in simulating the subsurface heat transfer and its influence on the unsaturated zone thermal dynamics (Section 3.3.2). Overall, producing groundwater variables, i.e. GWL and GT with satisfactory performance enabled a mechanistic assessment of groundwater contributions, in terms of mass and heat, to different soil and vegetation processes at the three sites as explained in the following subsections (Sections 4.1 - 4.4).

Although lateral groundwater flow was not simulated in the present 1D applications, its potential effect was indirectly accounted for by calibrating the ST-SC-MF6 models against the observed GWL. By adjusting aquifer parameters, so that simulated GWL closely matched observed ones, the 1D ST-SC-MF6 models implicitly incorporated the net outcome of lateral inflows, drainage, irrigation, and pumping on the GWL dynamics. Nevertheless, incorporating lateral groundwater flow in future 2D/3D applications would likely improve process realism, particularly when assessing groundwater as a managed water resource and its broader role in ecosystem functioning.



687

688 Figure 3. Comparison of half-hourly simulated groundwater level (GWL) and groundwater
689 temperature (GT) values by STEMMUS-SCOPE-MODFLOW 6 (blue lines) and observed ones (black
690 lines) during the calibration period (1 April 2016 – 31 March 2020) and the validation period (1 April
691 2020 – 31 March 2024; grey shaded) at: Loobos (a and b), Cabauw (c), and Veenkampen (d). Land
692 surface elevation values of the three sites are shown in Table 2

693 ## 3.3. Unsaturated zone dynamics

694 ### 3.3.1. Soil moisture

695 Figure 4 presents half-hourly observations and simulated outputs from the ST-SC and the ST-SC-MF6
696 models for θ at available depths at the three sites. The improvements in capturing the θ dynamics
697 within ST-SC-MF6 simulations were evident at all soil depths, but were most pronounced during the
698 wet periods at Cabauw and Veenkampen sites, characterized by shallow groundwater depths (0 -
699 1.25 m). At these two sites, the ST-SC-MF6 models successfully captured the θ peaks, occurred

Formatte
Italic

during winter periods, along different soil depths (0.6 m^3 m^{-3} at Cabauw and 0.75 m^3 m^{-3} at Veenkampen), representing near-saturation conditions. Those peaks reflect strong connectivity between soil and groundwater and the strong influence of groundwater on the soil profiles. In contrast, the ST-SC models underestimated these winter θ peaks, as the absence of groundwater limited the θ ability to reach saturation conditions. At Loobos, groundwater depth was relatively moderate (3 – 5 m), and had limited influence on the θ dynamics. Thus, the improvement of the θ simulation of the ST-SC-MF6 over the ST-SC model at Loobos was less associated with direct groundwater feedback and more related to improved parameter calibration within the ST-SC-MF6 model.

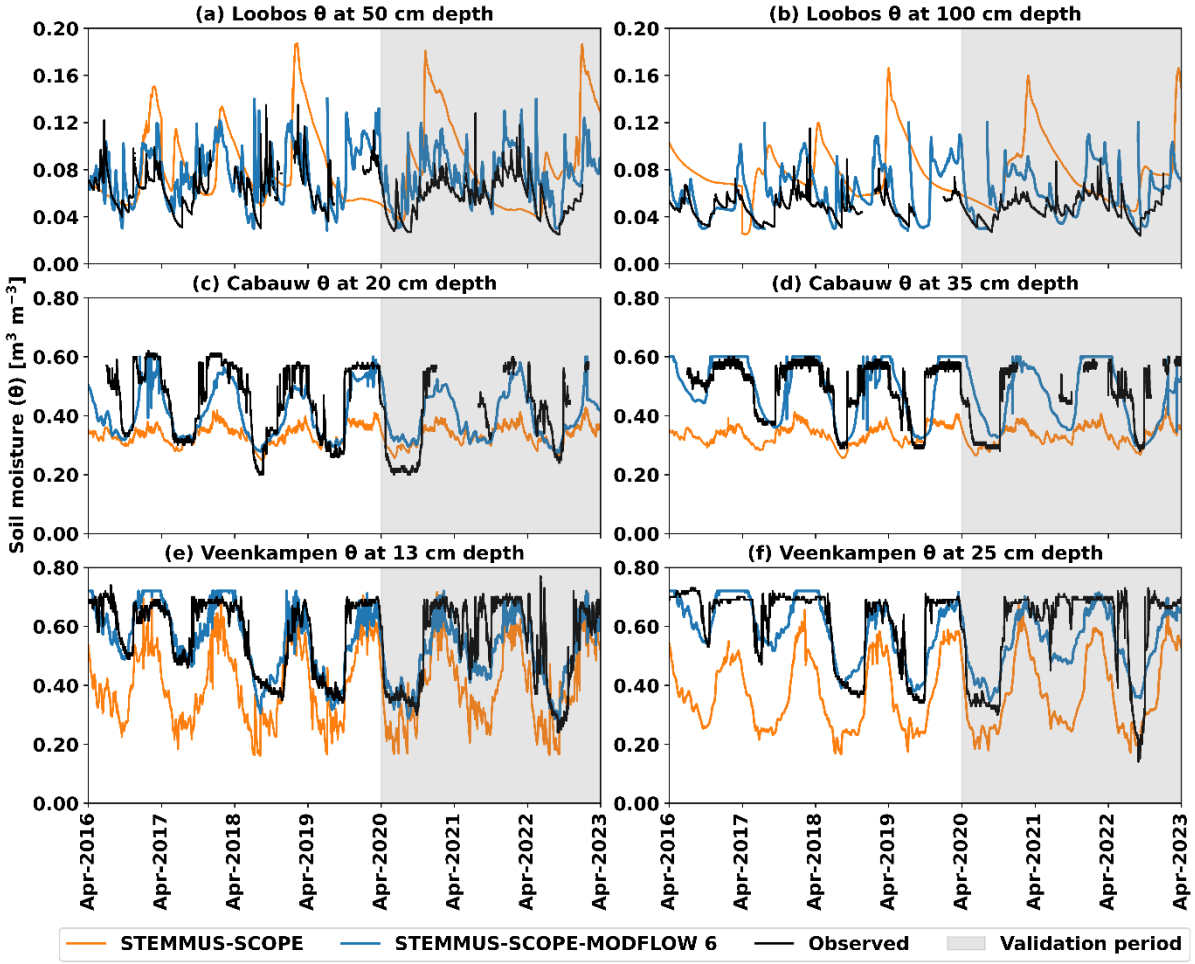


Figure 4 . Comparison of half-hourly simulated soil moisture (θ) values by STEMMUS-SCOPE (orange lines), by STEMMUS-SCOPE-MODFLOW 6 (blue lines), and observed ones (black lines) during the

calibration period (1 April 2016 – 31 March 2020) and the validation period (1 April 2020 – 31 March 2024; grey shaded) for: Loobos at depth: a) 50 cm, b) 100 cm; Cabauw at depth: c) 20 cm, d) 35 cm; and Veenkampen at depth: e) 13 cm, f) 25 cm

3.3.2. Soil temperature

Figure 5 presents half-hourly observations and simulated outputs from the ST-SC and the ST-SC-MF6 models for T_s at available depths at the three sites. The ST-SC-MF6 model showed a closer agreement with the observations than the ST-SC model at the three sites, but were more pronounced at Loobos. The GT observations were only available at Loobos, enabling a direct assessment of groundwater influence on T_s, unlike the case at Cabauw and Veenkampen. At Loobos, the ST-SC-MF6 simulation well captured the T_s dynamics (Figure 5~~Figure~~ a and b). In contrast, ~~T~~the ST-SC simulation showed an overestimation of the θ amplitude (fluctuations), which ~~affects~~reduced (dampen~~s~~ed) the T_s amplitude, leading to lower T_s peaks and higher T_s troughs than the observations. Similarly, ~~In contrast, the ST-SC-MF6 simulation well captured the θ amplitude~~at Cabauw, the ST-SC-MF6 simulation captured well the T_s dynamics, while in contrast, the ST-SC simulation showed an overestimation of the T_s amplitude, leading to higher T_s peaks and lower T_s troughs than the observations (Figure 5c and d). ~~but overestimated the T_s amplitude, resulting in higher T_s peaks and lower T_s troughs than the observed T_s.~~At Veenkampen,~~Regarding T_s,~~ both models generally reproduced the seasonal T_s patterns and corresponded well with the observations, but -exhibited a systematic tendency to slightly overestimate T_s amplitudes ~~except for the underestimated troughs by ST-SC-MF6~~ along the entire soil profiles (Figure 5e and f).

Formatte Calibri

Formatte Script For grammar

Formatte Calibri

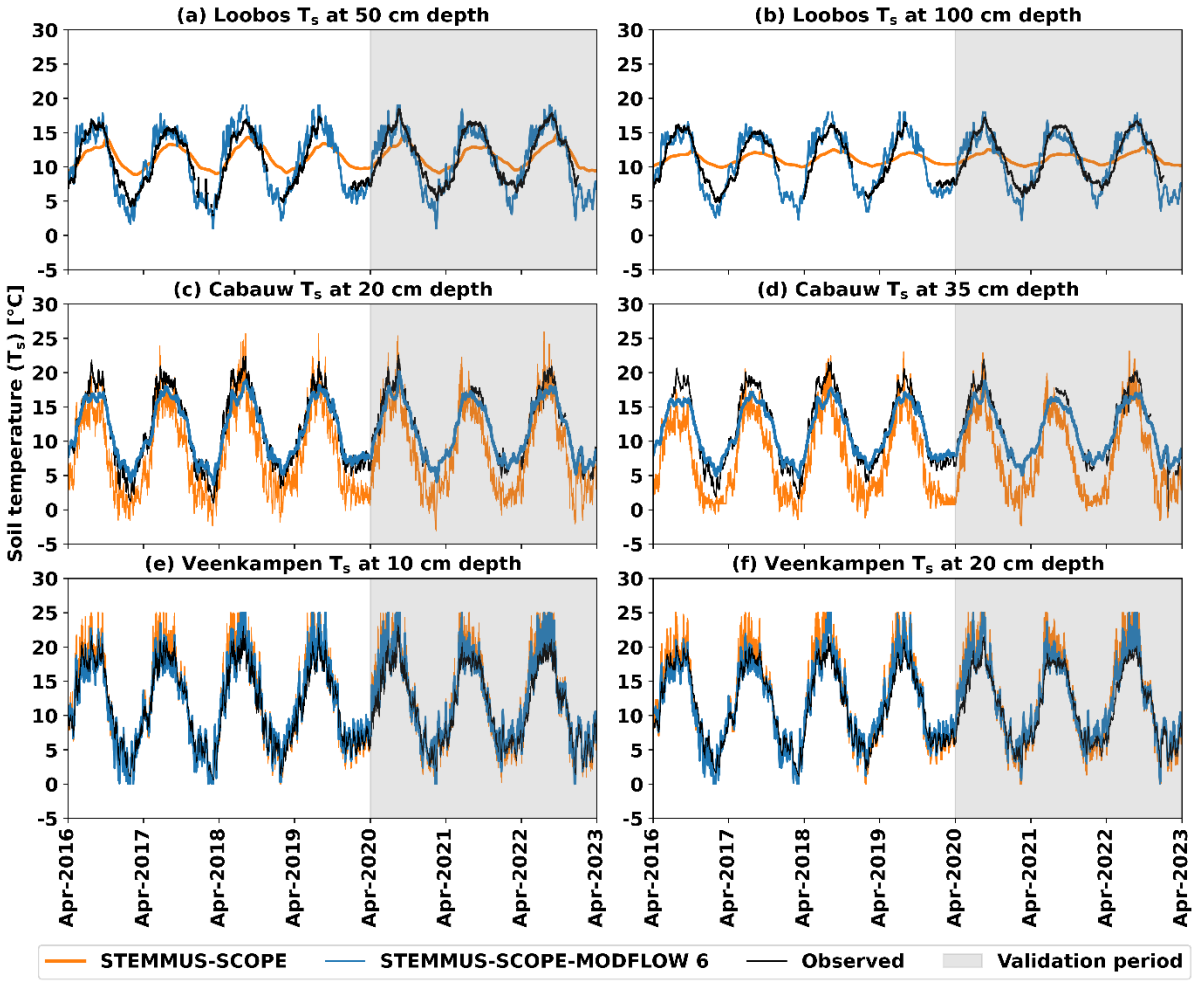
Formatte Script For grammar

Formatte Calibri

Formatte Script For grammar

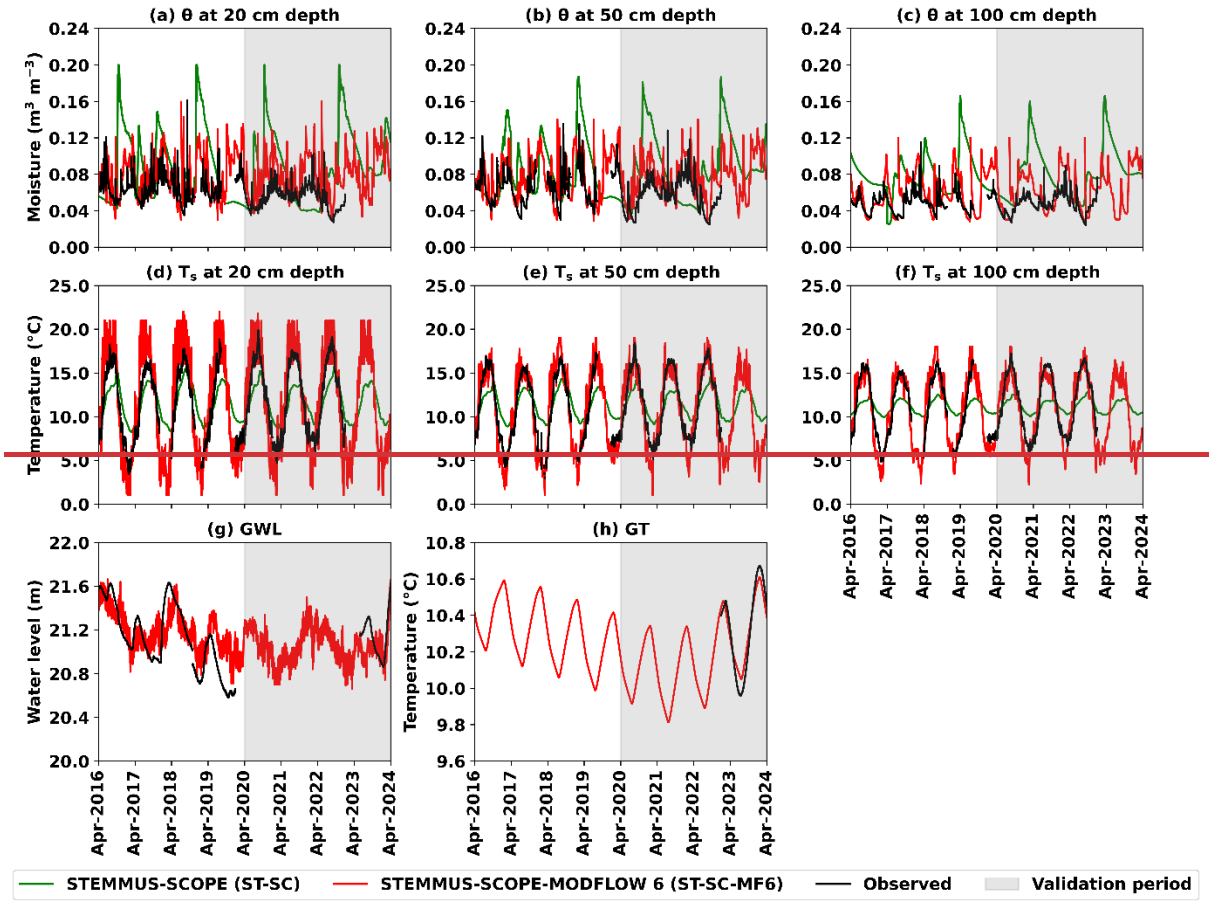
Formatte Calibri

Formatte Script For grammar



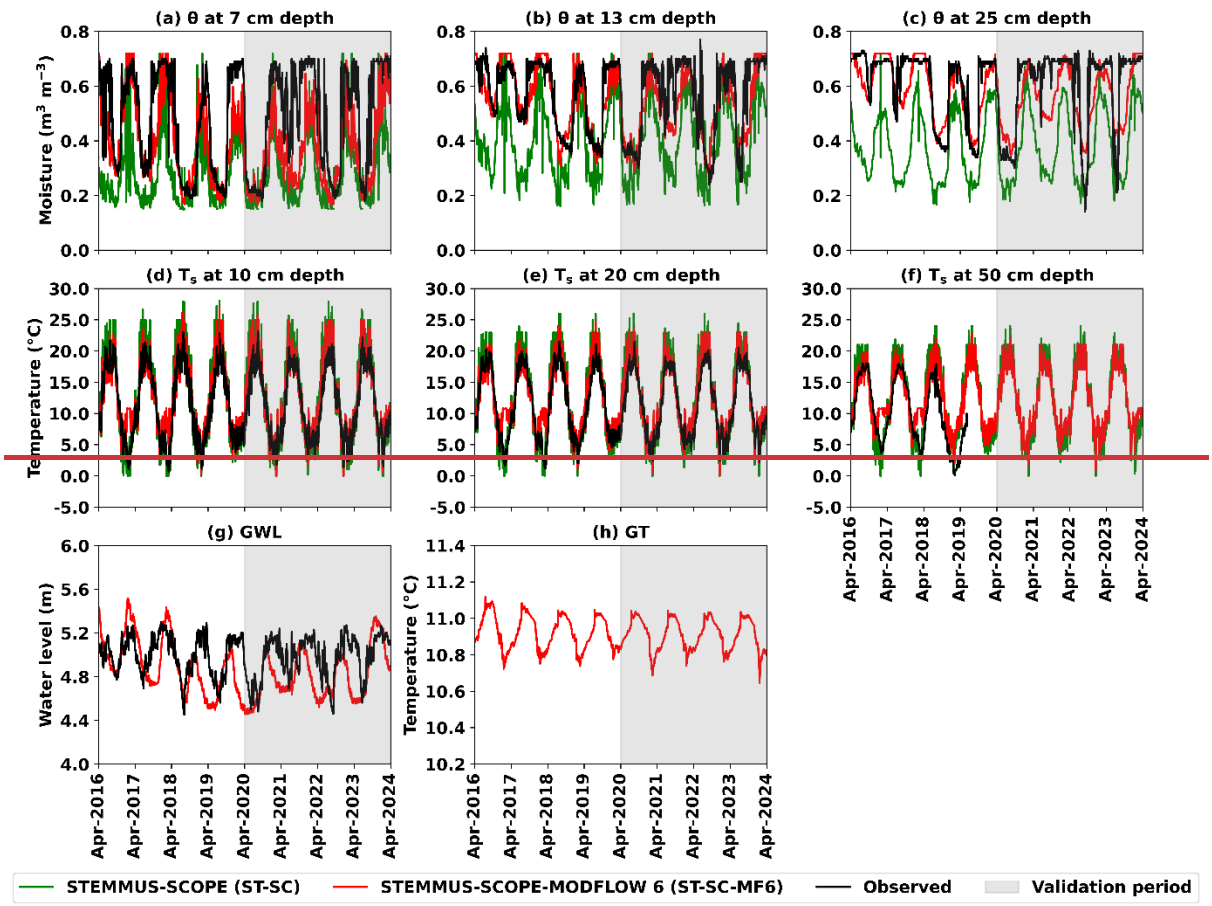
752

753 Figure 5. Comparison of half-hourly simulated soil temperature (T_S) values by STEMMUS-SCOPE
754 (orange lines), by STEMMUS-SCOPE-MODFLOW 6 (blue lines), and observed ones (black lines) during
755 the calibration period (1 April 2016 – 31 March 2020) and the validation period (1 April 2020 – 31
756 March 2024; grey shaded) for: Loobos at depth: a) 50 cm, b) 100 cm; Cabauw at depth: c) 20 cm, d)
757 35 cm; and Veenkampen at depth: e) 10 cm, f) 20 cm



~~*Figure 3. Loobos site – comparison of half-hourly simulated values by STEMMUS-SCOPE (green lines), by STEMMUS-SCOPE-MODFLOW 6 (red lines), and observed ones (black lines) during the calibration period (1 April 2016 – 31 March 2020) and the validation period (1 April 2020 – 31 March 2024; grey shaded) of the following: soil moisture (θ) at depths: a) 20 cm, b) 50 cm, c) 100 cm; soil temperature (T_s) at depths: d) 20 cm, e) 50 cm, f) 100 cm; (g) groundwater level (GWL), and h) groundwater temperature (GT)*~~

~~*Figure 5. Cabauw site – comparison of half-hourly simulated values by STEMMUS-SCOPE (green lines), by STEMMUS-SCOPE-MODFLOW 6 (red lines), and observed ones (black lines) during the calibration period (1 April 2016 – 31 March 2020) and the validation period (1 April 2020 – 31 March 2024; grey shaded) of the following: soil moisture (θ) at depths: a) 20 cm, b) 50 cm, c) 100 cm; soil temperature (T_s) at depths: d) 20 cm, e) 50 cm, f) 100 cm; g) groundwater level (GWL), and h) groundwater temperature (GT)*~~



~~*Figure 8. Veenkampen site – comparison of half-hourly simulated values by STEMMUS-SCOPE (green lines), by STEMMUS-SCOPE-MODFLOW 6 (red lines), and observed ones (black lines) during the calibration period (1 April 2016 – 31 March 2020) and the validation period (1 April 2020 – 31 March 2024; grey shaded) of the following: soil moisture (θ) at depths: a) 20 cm, b) 50 cm, c) 100 cm; soil temperature (T_s) at depths: d) 20 cm, e) 50 cm, f) 100 cm; (g) groundwater level (GWL), and h) groundwater temperature (GT)*~~

3.4. Evapotranspiration

Figure 6 illustrates daily observed and simulated ET from the ST-SC and ST-SC-MF6 models at the three sites. The zoom windows in Figure 6 highlight the results during a dry period example in the calibration period (1 June 2019 – 30 September 2019) and in the validation periods (1 June 2021 – 30 September 2021). Overall at the three sites, the ST-SC-MF6 models exhibited a better match with the ET observations, particularly during the dry periods, as compared to the ST-SC models. The ST-SC simulations showed rapid ET declines during the highlighted dry period examples, when precipitation declined, leading to θ limitation. In contrast, the ST-SC-MF6 simulations maintained

Formatte
Italic, Che
Formatte
Italic, Che

higher ET rates during those dry period examples due to the sustained water supply from groundwater. This buffering effect reduced underestimation of the simulated ET and better captured the observations.

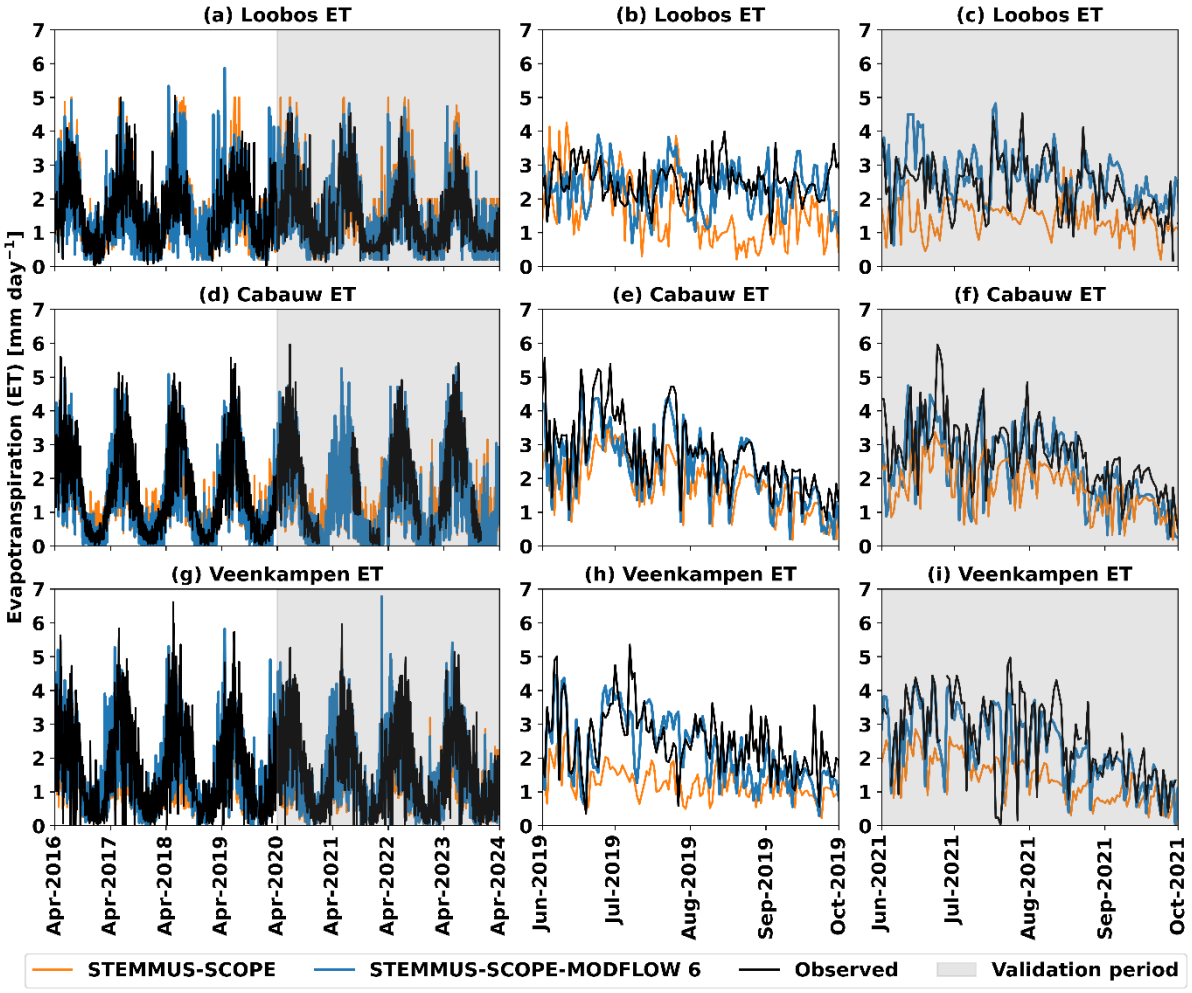
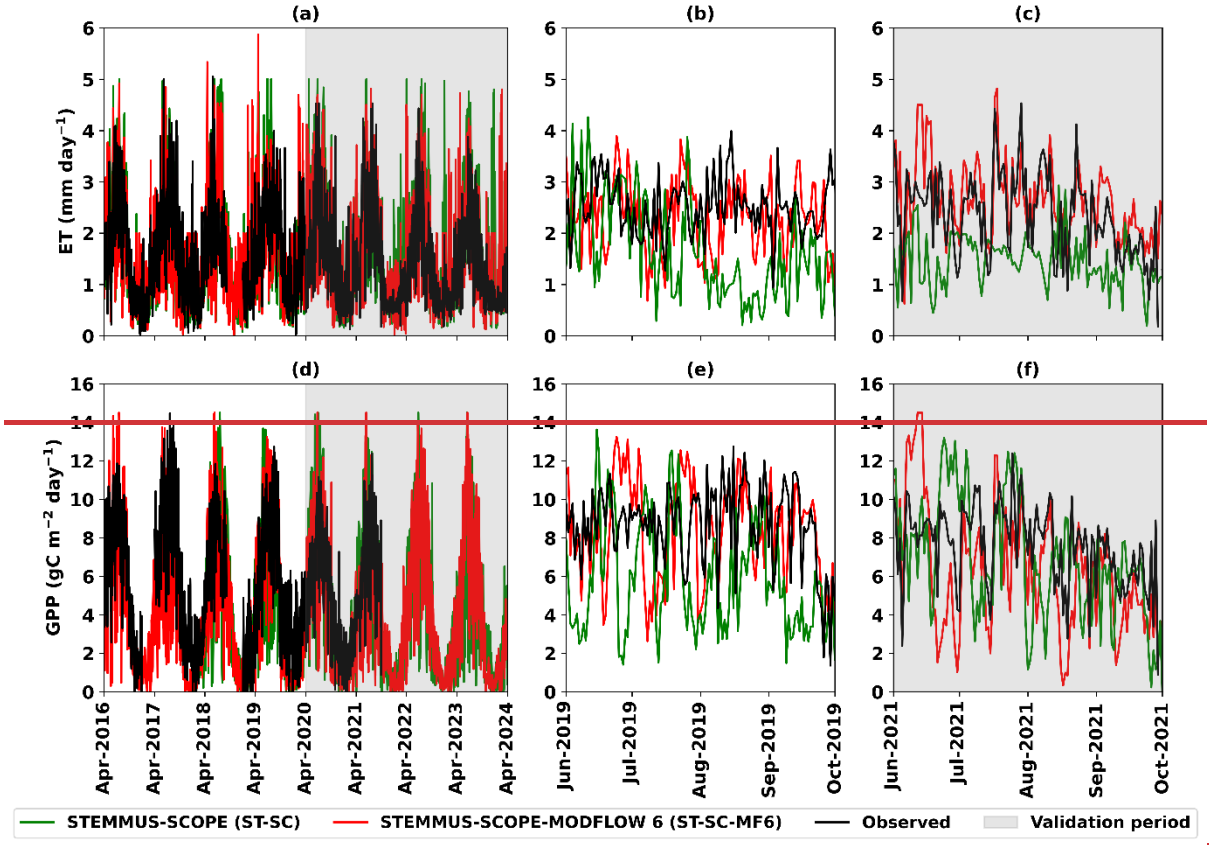
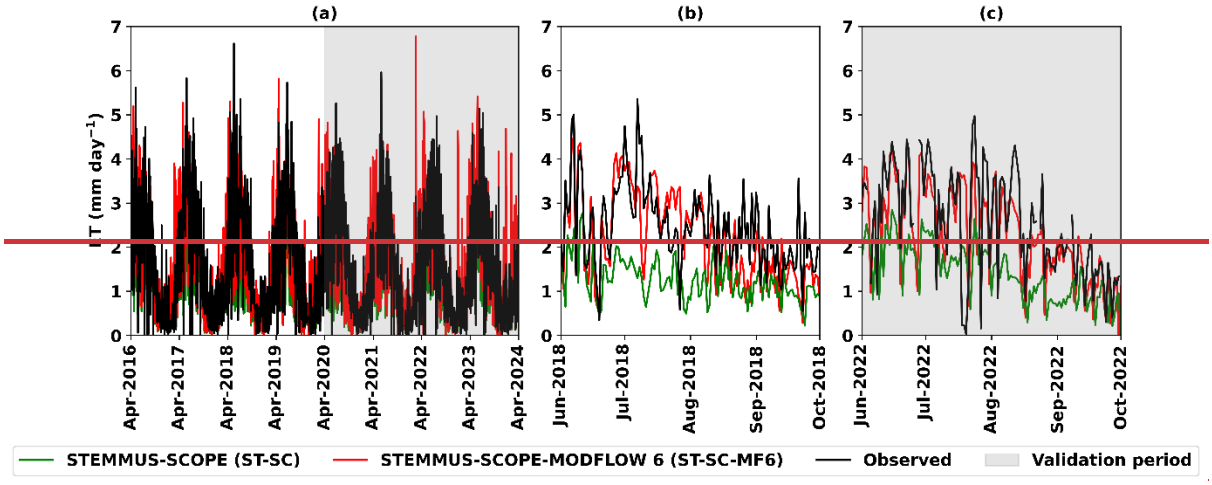


Figure 6. Comparison of half-hourly simulated evapotranspiration (ET) values by STEMMUS-SCOPE (orange lines), by STEMMUS-SCOPE-MODFLOW 6 (blue lines), and observed ones (black lines) during the calibration period (1 April 2016 – 31 March 2020) and the validation period (1 April 2020 – 31 March 2024; grey shaded) at: (a) Loobos, (d) Cabauw, (g) Veenkampen; with windows zooming (b, e, and h) in a dry period example in the calibration period (1 June 2019 – 30 September 2019), and (c, f,

and i) in a dry period example in the validation period (1 June 2021 –30 September 2021)



~~*Figure 4. Loobos site – comparison of daily simulated values by STEMMUS-SCOPE (green lines), by STEMMUS-SCOPE-MODFLOW 6 (red lines), and observed ones (black lines) during the calibration period (1 April 2016 – 31 March 2020) and the validation period (1 April 2020 – 31 March 2024; grey shaded) of the following: a) evapotranspiration (ET) with two windows zooming in: b) a dry period example in the calibration period (1 June 2019 – 30 September 2019), c) a dry period example in the validation period (1 June 2021 – 30 September 2021); d) gross primary productivity (GPP) with two windows zooming in the same dry periods in: e) the calibration period, and f) the validation period Figure 6. Cabauw site – comparison of daily simulated values by STEMMUS-SCOPE (green lines), by STEMMUS-SCOPE-MODFLOW 6 (red lines), and observed ones (black lines) during the calibration period (1 April 2016 – 31 March 2020) and the validation period (1 April 2020 – 31 March 2024; grey shaded) of the following: a) evapotranspiration (ET) with two windows zooming in: b) a dry period example in the calibration period (1 June 2018 – 30 September 2018), c) a dry period example in the validation period (1 June 2020 – 30 September 2020); d) net ecosystem exchange (NEE) with two windows zooming in the same dry periods in: e) the calibration period, and f) the validation period*~~



~~*Figure 9. Veenkampen site – comparison of daily simulated evapotranspiration (ET) by STEMMUS-SCOPE (green lines), by STEMMUS-SCOPE-MODFLOW 6 (red lines), and observed ones (black lines) during the calibration period (1 April 2016 – 31 March 2020) and the validation period (1 April 2020 – 31 March 2024; grey shaded) with two windows zooming in: (b) a dry period example in the calibration period (1 June 2018 – 30 September 2018), and (c) a dry period example in the validation period (1 June 2022 –30 September 2022)*~~

3.5. Carbon fluxes and SIF

Figure 7 illustrates daily observations and simulated carbon fluxes (GPP at Loobos and NEE at Cabauw) from the ST-SC and ST-SC-MF6 models, with zoom windows to highlight the results during a dry period example in the calibration period (1 June 2019 – 30 September 2019) and in the validation period (1 June 2020 –30 September 2020). At Loobos, groundwater influence on θ dynamics was weak, so GPP simulations were largely unchanged, and both ST-SC and ST-SC-MF6 models aligned well with the observations during the simulation period, including the dry periods (Figure 7b and c). While at Cabauw, where strong groundwater influence on θ dynamics was observed, the ST-SC-MF6 model demonstrated a better match with the NEE observations, particularly during the dry periods (Figure 7e and f), as compared to ST-SC.

Formatte
Italic

Formatte
Italic, Che

Formatte
Italic, Che

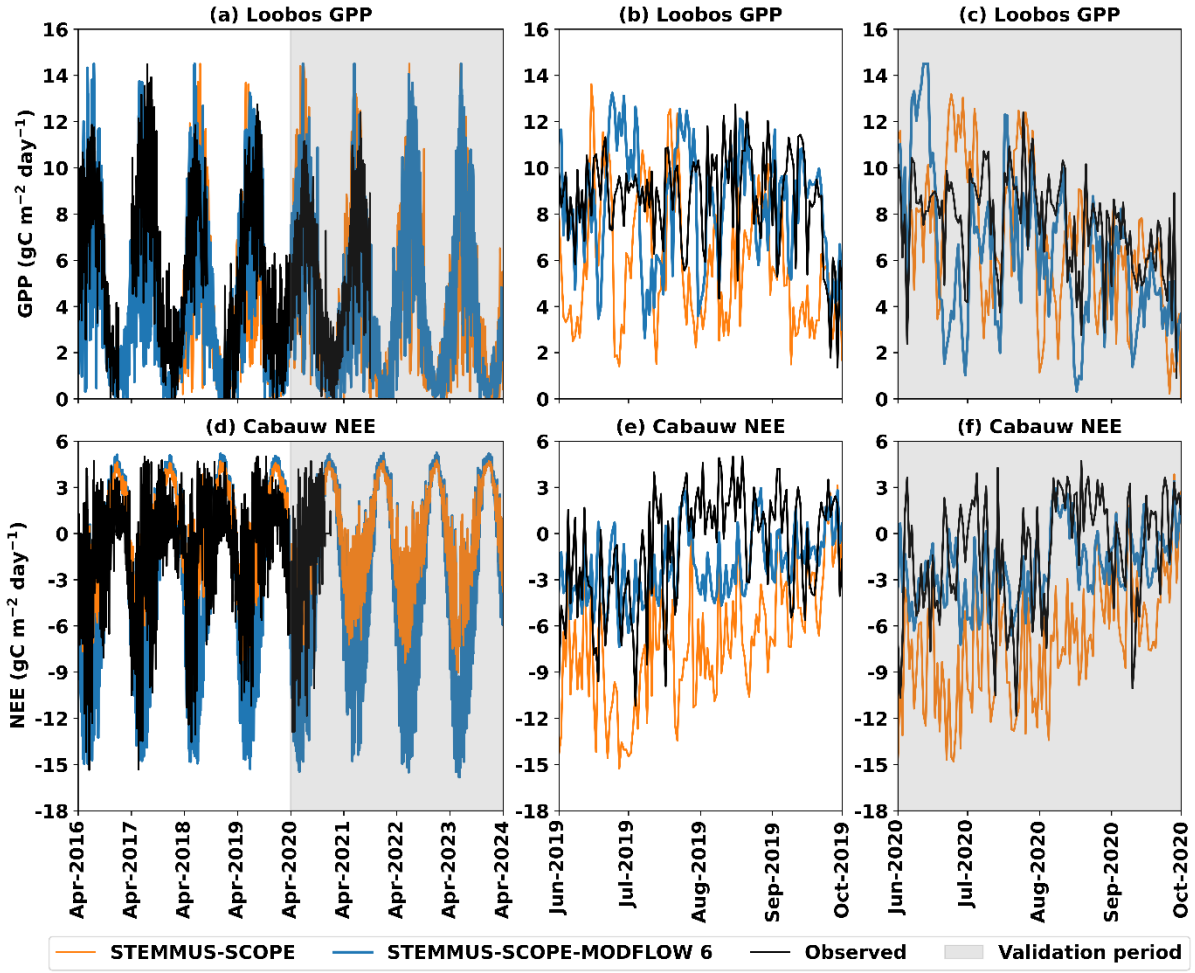


Figure 7. Comparison of half-hourly simulated carbon fluxes, i.e. gross primary productivity (GPP) and net ecosystem exchange (NEE) values by STEMMUS-SCOPE (orange lines), by STEMMUS-SCOPE-MODFLOW 6 (blue lines), and observed ones (black lines) during the calibration period (1 April 2016 – 31 March 2020) and the validation period (1 April 2020 – 31 March 2024; grey shaded) at: (a) Loobos, and (d) Cabauw; with windows zooming (b and e) in a dry period example in the calibration period (1 June 2019 – 30 September 2019), and (c and f) in a dry period example in the validation period (1 June 2020 –30 September 2020)

Figure 8 shows half-hourly observations and simulated SIF from ST-SC and ST-SC-MF6 on certain days at Cabauw, when the observed SIF data were available. During the summer days 9–14 August 2022 (Figure 8a), the ST-SC-MF6 demonstrated a better agreement with the SIF observations as compared to the ST-SC. Both models aligned well with the observations during the days 3–6 June 2023 (Figure

8c), which were dry days (Figure 4c and d), while both models underestimate the SIF in the winter days 12–15 November 2022 (Figure 8b).

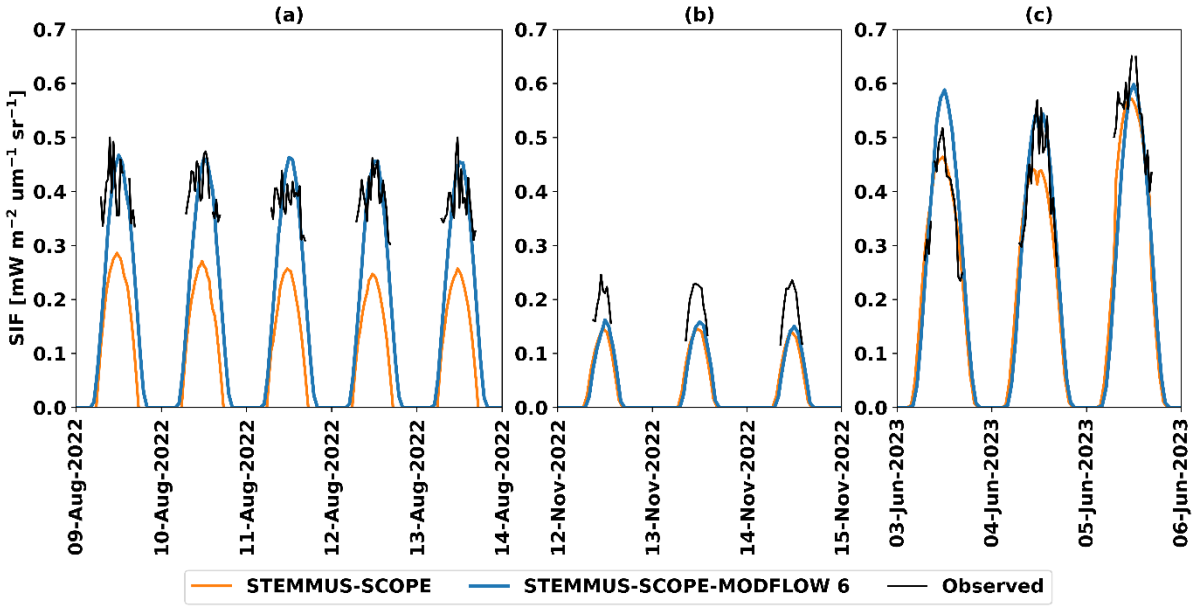


Figure 8. Cabauw site – comparison of half-hourly simulated sun-induced chlorophyll fluorescence (SIF) by STEMMUS-SCOPE (orangegreen lines), by STEMMUS-SCOPE-MODFLOW 6 (bluered lines), and observed ones (black lines) during the days: a) 9 August 2022 – 14 August 2022, b) 12 November 2022 – 15 November 2022, and c) 3 June 2023 – 6 June 2023

~~Figure 3 presents half-hourly observations and simulated outputs from the ST-SC and the ST-SC-MF6 models of the following: θ at depths 20, 50, and 100 cm (Figs. 3a, b, c); T_s at the same depths (Figs. 3d, e, f); GWL (Fig. 3g), and GT (Fig. 3h). The ST-SC-MF6 simulation of θ and T_s showed substantial improvement over ST-SC, during both the calibration and the validation periods. The ST-SC simulation showed an overestimation of the θ amplitude (fluctuations), which inversely affects (dampens) the T_s amplitude, leading to lower T_s peaks and higher T_s troughs than the observations. In contrast, the ST-SC-MF6 simulation well captured the θ amplitude but overestimated the T_s amplitude, resulting in higher T_s peaks and lower T_s troughs than the observed T_s. The KGE values of θ at depths 20, 50, and 100 cm were 0.29, 0.46, 0.18 (Table 4) with corresponding RMSE values of 0.03, 0.02, 0.02 $m^3 m^{-3}$ (Table 5) for the ST-SC-MF6, as compared to KGE values equal to 0.02, 0.01,~~

~~0.02, and RMSE values equal to 0.05, 0.04, 0.04 $m^3 m^{-3}$ for the ST-SC, respectively. For T_s at the same depth, the ST-SC-MF6 yield KGE values of 0.49, 0.49, 0.56 (Table 4), with RMSE values of 1.73, 1.41, 1.72 °C (Table 5), as compared to KGE values equal to 0.42, 0.33, 0.22, and RMSE values equal to 2.39, 2.36, 2.73 °C for the ST-SC, respectively. Besides, the simulated GWL and GT by ST-SC-MF6 (Figs. 3g and h) showed a good match with the observations, with KGE values equal to 0.26 and 0.56 (Table 4), and RMSE values equal to 0.49 m and 0.17 °C (Table 5), respectively.~~

~~Table 5. KGE values of the state variables for the STEMMUS-SCOPE (ST-SC) and STEMMUS-SCOPE-MODFLOW 6 (ST-SC-MF6) models at the three sites over the entire period simulationTable 6. RMSE values of the state variables for the STEMMUS-SCOPE (ST-SC) and STEMMUS-SCOPE-MODFLOW 6 (ST-SC-MF6) models at the three sites over the entire period simulation~~

~~Cabauw site~~

~~Figure 5 presents half-hourly observations and simulated outputs from ST-SC and ST-SC-MF6 models of the following: θ at depths 20, 35, and 55 cm (Figs. 5a, b, c); T_s at the same depths (Figs. 5d, e, f); GWL (Fig. 5g), and GT (Fig. 5h). The ST-SC-MF6 simulation of θ demonstrated improved agreement with the observations during both the calibration and the validation periods, as compared to the ST-SC simulation. The KGE values of θ at depths 20, 35, and 55 cm was improved to 0.7, 0.57, 0.55 for ST-SC-MF6, as compared to 0.29, 0.37, 0.49 for ST-SC, respectively (Table 4). The RMSE values of θ at the same depths were reduced to 0.08, 0.1, 0.08 $m^3 m^{-3}$ for ST-SC-MF6, as compared to 0.14, 0.17, 0.18 $m^3 m^{-3}$ for ST-SC, respectively (Table 5). Regarding T_s, both models generally correspond well with the observations except for the underestimated troughs by ST-SC-MF6 along the entire soil profile (Figs. 5d, e, and f). Both KGE and RMSE values of T_s at depths 20, 35, and 55 cm for both models were close to each other (Table 4 and 5). The KGE values were 0.84, 0.67, 0.78 for ST-SC-MF6 and 0.85, 0.76, 0.64 for ST-SC, respectively and the RMSE values were 1.6, 1.4, 1.6 °C for ST-SC-MF6 and 1.2, 1.4, 1.7 °C for ST-SC, respectively. Additionally, the ST-SC-MF6 simulated GWL showed a~~

~~good match with the observations (Table 4 and 5), with KGE values equal to 0.63 and RMSE values equal to 0.21 m (Fig. 5g).~~

~~Figure 6 illustrates daily observations and simulated ET and NEE from ST-SC and ST-SC-MF6 models. The zoom windows in Figs. 6b, c, e, and f emphasize the results during a dry period example in the calibration period (1 June 2018 – 30 September 2018) and in the validation period (1 June 2020 – 30 September 2020). The ST-SC-MF6 model exhibited a closer agreement with the ET observations, particularly during the dry periods (Figs. 6b and c), as compared to ST-SC. The KGE and RMSE values were improved to 0.76 and 0.76 mm day^{-1} for ST-SC-MF6, as compared to 0.65 and 0.95 mm day^{-1} for ST-SC, respectively (Table 4 and 5). Similarly, for NEE, the ST-SC-MF6 model demonstrated a better match with the NEE observations, particularly during the dry periods (Figs. 6e and f), as compared to ST-SC. The KGE and RMSE values were improved to 0.19 and 4.46 gC m^{-2} day^{-1} for ST-SC-MF6, as compared to 0.01 and 7.0 gC m^{-2} day^{-1} for ST-SC, respectively (Table 4 and 5).~~

~~Figure 7 shows half-hourly observations and simulated SIF from ST-SC and ST-SC-MF6 on certain days, when the observed SIF data were available. During the summer days 9–14 August 2022 (Fig. 7a), the ST-SC-MF6 demonstrated an improved agreement with the SIF observations. Both models aligned well with the observations during days 3–6 June 2023 (Fig. 7c), which were dry days (Figs. 5a, b, and c), while both models underestimate the SIF in the winter days 12–15 November 2022 (Fig. 7b).~~

~~Veenkampen site~~

~~Figure 8 presents half-hourly observations and simulated outputs from ST-SC and ST-SC-MF6 models of the following: θ at depths 7, 13, and 25 cm (Figs. 8a, b, c); T_s at depths 10, 20, and 50 cm (Figs. 8d, e, f); GWL (Fig. g), and GT (Fig. 8h). The ST-SC-MF6 simulation of θ showed a better agreement with the observations during both the calibration and the validation periods, as compared to the ST-SC simulation (Figs. 8a, b, c). The KGE values of θ at depths 7, 13, and 25 cm were improved to 0.53, 0.82, and 0.71 for ST-SC-MF6, as compared to 0.49, 0.42, and 0.26 for ST-SC, respectively (Table 4).~~

~~The RMSE values of θ at the same depths were reduced to 0.12, 0.08, 0.09 $m^3 m^{-3}$ for ST-SC-MF6, as compared to 0.24, 0.19, 0.25 $m^3 m^{-3}$ for ST-SC, respectively (Table 5). Regarding T_s, both models generally correspond well with the observations except for the overestimated peaks along the entire soil profile (Figs. 8d, e, and f). Both KGE and RMSE values of T_s at depths 10, 20, and 50 cm for both models were close to each other (Table 4 and 5). The KGE values were 0.86, 0.84, 0.53 for ST-SC-MF6 and 0.72, 0.83, 0.77 for ST-SC, respectively, and the RMSE values were 2.1, 2.2, 2.5 °C for ST-SC-MF6 and 2.5, 2.2, 2.9 °C for ST-SC, respectively. Additionally, the ST-SC-MF6 simulated GWL showed a good match with the observations (Table 4 and 5), with KGE values equal to 0.37, and RMSE values equal to 0.26 m (Fig. 8g).~~

4. Discussion

~~The main objective of this study was to better understand what impact a more robust representation of groundwater has on modelling the soil-plant-atmosphere continuum. We hypothesized that explicitly representing groundwater mass and energy would improve modelling the soil-plant-atmosphere continuum. To achieve this, an IEM framework was developed by coupling the STEMMUS-SCOPE SPAC model to the MODFLOW 6 IHM. The coupling was implemented using the BMI coupling approach (Peckham et al., 2013; Hutton et al., 2020). The BMI approach was followed because it facilitates the coupling at the shared interface between the respective models by exchanging the models' calculated variables through memory; thereby eliminating the need to modify the source code of either model. Hence, BMI allows for keeping up with advances of the individual models. Additionally, using BMI, the coupled models are run through executable files without the need to access the source code of the models during the models' simulation. Thus, BMI allows for coupling models that are written in different programming languages, as exemplified in this study (STEMMUS-SCOPE in MATLAB and MODFLOW 6 in Fortran).~~

The ST-SC-MF6 IEM was tested at ~~3~~ three different sites (the Loobos forest, the Cabauw and Veenkampen meadow sites) in the Netherlands. Different key variables from the water, energy, and carbon cycles were analyzed for the two simulations (with and without coupling with MODFLOW 6) – namely, θ, T_s, GWL, GT, ET, GPP, NEE, and SIF. ~~Comparing results (section 3) from the ST-SC and ST-SC-MF6 simulations highlights the~~ The benefits of representing the groundwater in model~~ls of~~ing ~~soil-plant-atmosphere continuum~~the SPAC processes~~.~~ are described in the following subsections.

4.1. Effect of groundwater on ~~the~~ soil moisture ~~profile~~

The benefits obtained from incorporating groundwater within ST-SC-MF6 comes from the role changes that groundwater plays in the processes simulation. The GWL, simulated by MODFLOW 6, was used as a bottom boundary for the soil water module in STEMMUS-SCOPE; thereby influencing the $\psi_{s,i}$ and θ profiles. In the capillary fringe zone, above the GWL, soil is nearly saturated, causing the $\psi_{s,i}$ to become less negative, and the corresponding θ to increase significantly. Moving upward to the soil surface, the influence of the GWL gradually diminishes, and other surface forces (i.e. precipitation) become the dominant driver of $\psi_{s,i}$ and θ in the upper soil layers. However, the extent to which the GWL affects $\psi_{s,i}$ and θ depends on the thickness of the unsaturated zone, where groundwater fluctuations occur. When the water table is shallow, its influence can extend upward beyond the lower soil layers, affecting the upper profile with decreasing intensity. Then, over time, as GWL rises, the entire $\psi_{s,i}$ profile shifts towards less negative and θ increases throughout the entire soil profile. Conversely, a falling GWL leads to a more negative $\psi_{s,i}$ profile and a decrease in θ.

The impact of groundwater on the θ profile was particularly evident at Cabauw and Veenkampen sites, where groundwater depths were shallow (from 0 to 1.25 m below land surface). At these two sites, the strong hydraulic connectivity between the phreatic surface and the unsaturated zone enabled the GWL fluctuations to propagate upward through the soil profile, directly regulating the θ dynamics. The ST-SC-MF6 models improved the representation of the seasonal θ variability by dynamically resolving this connectivity. During winter wet periods (December - March), the θ

variability is primarily controlled by groundwater fluctuations (McMillan & Srinivasan, 2015). This was observed in the simulations by the rise of the GWL (Figure 3c and d), associated with the increase of the θ towards the observed θ peaks (0.6 m^3 m^{-3} at Cabauw and 0.75 m^3 m^{-3} at Veenkampen), approaching near-saturation conditions (Figure 4c, d, e and f). In spring periods (April – June), when vegetation is mainly active, enhanced RWU_s progressively depleted the θ, while GWL is still relatively high. Further towards summer dry periods (July – September), limited or no precipitation reduced the R_g, leading to GWL decline and the development of a drier soil profile (Gao et al., 2017; Li et al., 2017) with minimum θ values of 0.2 m^3 m^{-3} at Cabauw and 0.15 m^3 m^{-3} at Veenkampen, respectively (Figure 4c, d, e and f).

~~In the Cabauw and Veenkampen sites, the groundwater depth is shallow (from 0 to 1.5 m below land surface); thus, the GWL had a significant impact on the θ profile. The GWL contribution is highlighted by a significantly improved match between the observed θ and the ST-SC-MF6 simulated one. By contrast, ST-SC underestimated the θ profile at the two sites (Figs. 5a, b, c and Fig. 8a, b, c).~~

At the Loobos site, the GWL impact on the θ profile was not ~~visible~~ evident. That can be attributed to two main factors. ~~because: 1)~~ First, the ~~Loobos~~ site ~~has~~ is characterized by a loamy sandy soil with a relatively low maximum observed θ (~ 0.16 m^3 m^{-3}) along the entire profile (Figure 4a and b), indicating limited specific retention capacity. Second, ~~and potentially 2)~~ the groundwater depth was relatively ~~deep~~ moderate (3 – 5 m below land surface), as compared to the other two sites. However, whether groundwater influence becomes negligible at depths between 3 and 5 m cannot be generalized from the Loobos site alone. ~~However, confirming that the GWL impact on the θ profile is minor in cases where the groundwater depth ranges between 3 and 5 m needs further investigation.~~ An experimental study by Zhao et al. (2023), conducted in a semi-arid region, showed that the θ within the upper 2 m of sandy soil increased with soil depth at 6 and 10 m groundwater depths, whereas there was no significant impact on θ at groundwater depth of 15 m. These findings, unlike the case in Loobos, suggest that the extent of the critical groundwater depth, which can still influence the θ is site dependant and strongly controlled by soil hydraulic properties. Therefore, ~~That~~

Formatte
Italic, Che

Formatte
Italic, Che

Formatte
Italic, Che

~~could be done in the~~ future ~~by~~ testing at different sites with similar groundwater depths (3 to 5 m) but different soil characteristics ~~with generally higher θ~~ than the Loobos site is further required. Nevertheless, the ST-SC models at the three sites were unable to reproduce the observed amplitude and seasonal variability of θ (Figure 4). That is because the absence of dynamic groundwater feedback prevented realistic representation of key interacting groundwater processes, i.e. R_g, RWU_s and RWU_g and their combined influence on θ.

4.2. Effect of groundwater on soil temperature

Groundwater energy and mass, represented by GWL and GT, showed effects on the T_s as discussed in the following subsections

~~4.1.1.~~4.2.1. Effect of groundwater temperature on soil temperature

~~Similarly, t~~The GT, simulated by MODFLOW 6, was used as a bottom boundary for the STEMMUS-SCOPE soil energy module. At Loobos, where GT observations were available, the ST-SC-MF6 produced a better simulation of the T_s profile as compared to the ST-SC (Figure 4a and b). At this site, the groundwater depth is relatively moderate (3 – 5 m below land surface), resulting in a balance between atmospheric and groundwater heat processes influencing on T_s. While the shallower soil layers closely follow atmospheric conditions, deeper layers are more influenced by groundwater conditions (Parrales et al., 2026). Both observed and simulated GT fluctuated between 10.6 °C during winter periods and 9.8 °C during summer periods (Figure 3b). In contrast, T_s exhibited a much a larger seasonal variability (Figure 4a and b), with both observed and simulated T_s ranging from 15.0 – 18.0 °C during summer period to 5.0 – 8.0 °C during winter period across the soil profile. With increasing soil depth, the T_s is damped with a seasonal phase lag until gradually approaching stable GT values. By incorporating the simulated GT as a bottom boundary condition for the unsaturated zone, the ST-SC-MF6 simulation successfully reproduced the same patterns as the observed T_s. During winter periods, the GT was higher than T_s, generating upward heat transfer by

Formatte
Italic, Che

Formatte
Italic, Che

Formatte
Italic, Che

diffusion, i.e. temperature gradient, from the saturated to the unsaturated zone. Towards the spring period (April – June), GT gradually declined, while T_s increased, resulting in a temporary equilibrium state between the two thermal regimes. Later during summer periods, the opposite situation occurs, with T_s exceeded GT, reversing the direction of the heat transfer from the unsaturated to the saturated zone.

It is notable that matching the simulated T_s with the corresponding observations at the Loobos site was challenging. The Loobos site has low values of θ (maximum value = 0.16 m^3 m^{-3}) along the soil profile (Figure 4a and b), corresponding with relatively low T_s values (maximum value = 18.0 °C). Such a situation created extra difficulty to be modelled, since in STEMMUS-SCOPE, the θ and T_s are simulated together with many influencing factors as follows: 1) the low θ may shift the energy partitioning to more sensible heat and less latent heat, which leads to low values of evaporation and extra soil warming (overestimation of T_s profile); and 2) the thermal parameterization (thermal ~~hydraulic~~ conductivity and heat capacity) in STEMMUS-SCOPE follows the de Vries ~~method~~ formulation (Yu et al., 2018), which is influenced by θ. In this case, the low θ values lowered the values of thermal parameters, which may lead to rapid soil heating and further contribute to the overestimation of T_s. Hence, the overestimation of the θ amplitude by ST-SC dampened the amplitude of the T_s.

Formatte
Italic, Che

4.2.2. Effect of groundwater level on soil temperature

At Cabauw and Veenkampen, although no GT observations were available to control the simulations, groundwater still exerted potential influence on T_s profile, driven by the GWL rather than the GT. The shallow groundwater depths (0.25 – 1 m below land surface) at these two sites enhanced soil thermal conductance and heat capacity, which facilitated heat transfer between the top soil and the subsurface (Alkhaier et al., 2012).Under such conditions, the unsaturated zone becomes more thermally connected to the atmospheric forcing rather than the saturated zone. Previous studies have reported strong correlation between GWL and T_s, particularly under shallow

groundwater depths, i.e. < 5 m (Alkhaier et al., 2012; Malik et al., 2021; Mandal & Roy, 2024; Oishy et al., 2025). The de Vries heat transport formulation, implemented in the energy module of STEMMUS-SCOPE (Yu et al., 2018), allows for producing such GWL – T_s relationship.

At Cabauw, the ST-SC-MF6 model showed a better simulation of the T_s profile as compared to the ST-SC model (Figure 5c and d). During winter periods, the GWL raised (Figure 3c), which was associated with high θ values, i.e. 0.6 m^3 m^{-3}, (Figure 4c and d) nearly approaching saturation, and relatively low T_s (Figure 5c and d). Nevertheless, both θ and T_s of the ST-SC-MF6 remained higher than the ones, produced by the ST-SC model and closer to the observed ones. During summer periods, the GWL declined, leading to low θ and high T_s values, while T_s remained higher than the values produced by the ST-SC model. Collectively, during the hydrological year, the presence of the shallow GWL in the ST-SC-MF6 simulation increased the seasonal amplitude of θ, i.e. raising maximum θ during winter while maintaining nearly similar minimum θ at summer. This behaviour, in turn, reduced the seasonal amplitude of T_s, i.e. increasing minimum T_s during winter and reducing maximum T_s during summer. In contrast, the ST-SC model, due to the absence of GWL, underestimated the θ amplitude and consequently overestimated the T_s amplitude.

At Veenkampen, the groundwater showed little impact on the T_s simulation (Figure 5e and f). This is likely because the ST-SC-MF6 model only slightly improved the θ simulation as compared to the ST-SC model. As a result, the thermal properties of the soil remained similar in both simulations, leading to comparable T_s dynamics. Additionally, in both models, the amplitude of the simulated T_s was slightly overestimated. The likely reason is the resistance scheme in the soil energy module in STEMMUS-SCOPE, which follows the big leaf concept, assuming that the boundary layer resistance is the same for all canopy layers – a simplification that could be refined in the future. ~~Using the calculated GT values improved the ST-SC simulation of the T_s profile for the Loobos site (Figs. 3d, e, and f).~~

Formatte Italic, Che

Formatte Italic, Che

Formatte Italic, Che

Formatte Italic, Che

4.2.3. Effect of groundwater on surface soil temperature and canopy temperature

Beyond the groundwater influence on T_s dynamics, groundwater can also affect the thermal regime of the land surface and vegetation canopy. These effects may propagate upward, influencing surface soil temperature (T_{ss}) and canopy temperature (T_c), which in turn regulate vegetation physiological processes such as stomatal conductance and carbon assimilation.

At Loobos, the groundwater – soil heat exchanges, simulated by the ST-SC-MF6 model, facilitated proper simulating of temperature dependent processes within the SPAC. In particular, the role the GT played to cool down the T_s, especially in the deeper soil layers, close to the capillary fringe zone, thereby stabilizing the root-zone thermal conditions and supporting the RWU_g – as been observed through the increase of RWU_g, simulated by ST-SC-MF6 (Section 4.3.3). Furthermore, the moderating influence of the GT on the T_s propagated upward to cool down T_{ss} and T_c. The ST-SC-MF6 simulation produced consistently cooler T_{ss} and T_c (i.e. lower peaks) during the spring periods compared to the ST-SC simulation, with reductions of approximately 1 °C in T_{ss} (Figure 9a and c) and up to 2 °C in T_c (Figure 9b and d).

At Cabauw, the influence of groundwater on the surface thermal regime is primarily controlled by the shallow GWL rather than GT. The shallow GWL moderates near-surface thermal conditions through its control on soil moisture and thermal properties; enhancing the buffering of temperature fluctuations in the soil profile. The ST-SC-MF6 simulation produced cooler T_{ss} (i.e. lower peaks, Figure 9e and g) and T_c (Figure 9f and h) during the spring periods as compared to the ST-SC simulation, with average reductions of about 1 °C and 2 °C, respectively. Such moderation of T_c, particularly during the spring periods, when the vegetation activity is high, would maintain stomatal conductance and support carbon uptake. Under good nutrient and water availability conditions, slightly cooler T_{ss} and T_c would further enhance photosynthesis and carbon assimilation (Oishy et al., 2025), as been observed in the NEE, simulated by ST-SC-MF6 (Section 4.4).

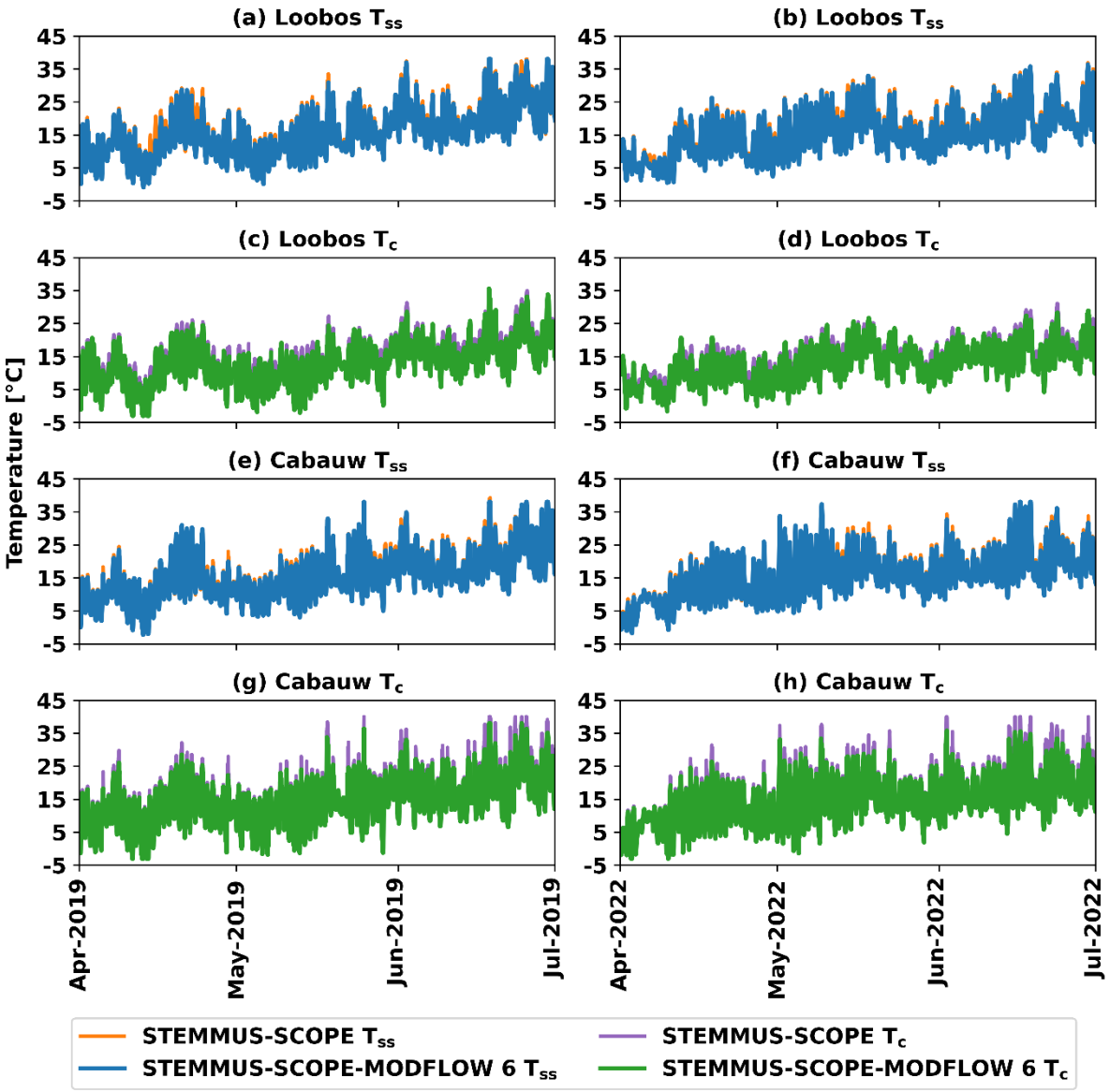


Figure 9. Comparison of half-hourly simulated surface soil temperature (T_{ss}) by STEMMUS-SCOPE (orange lines), by STEMMUS-SCOPE-MODFLOW 6 (blue lines), simulated canopy temperature (T_c) by STEMMUS-SCOPE (purple lines), by STEMMUS-SCOPE-MODFLOW 6 (green lines) in a spring period example in the calibration period (1 April 2019 – 30 June 2019) for Loobos (a and c) and Cabauw (e and g), and in the validation period (1 April 2020 –30 June 2020) for Loobos (b and d) and Cabauw (f and h)

~~4.2.~~4.3. Effect of groundwater on evapotranspiration components ~~water fluxes~~

~~Incorporating the simulated GWL and GT by MODFLOW 6 as bottom boundaries in STEMMUS-SCOPE allowed for: 1) calculating the R_g, R_n and Cap fluxes (Eq. 2); and 2) proper simulation of the Q_{heat} and RT_g. The R_n, Q_{heat} and RT_g were then fed back into MODFLOW 6 to update the GWL and GT for the next time step. Allowing the two models to exchange simulated values contributed to a proper representation of the dynamics between the unsaturated and saturated zones and resulted in: i) a good match between the simulated and observed GWL (KGE = 0.26, 0.63, 0.37 and RMSE = 0.49, 0.21, 0.26 m, respectively) at the 3 sites (Figs. 3g, 5g, and 8g), ii) a good match between the simulated and observed GT (KGE = 0.56 and RMSE = 0.17 °C) at the Loobos site (Fig. 3h), iii) more accurate simulation of θ and T_s, and in so doing iv) improved the simulation of other variables such as ET, carbon fluxes (GPP and NEE), and SIF variables as discussed below.~~

~~The groundwater showed a significant impact on simulated ET, which can be attributed to three reasons.~~ The explicit representation of groundwater improved the simulation of the ET. As shown in Figure *6*, the ST-SC-MF6 simulations generally reproduced the observed ET dynamics better than the ST-SC simulations, particularly during dry periods when groundwater contributed to sustaining θ and RWU. The improved ET representation originates from the more realistic simulation of individual ET components, i.e. E_{ss}, RWU_s, and RWU_g, which are discussed below.

4.3.1. Subsurface evaporation

~~Second,~~ At Cabauw and Veenkampen, the E_{ss} values simulated by ST-SC-MF6 models were increased by 7.3 and 12.6%, respectively as compared to the ST-SC models. These increases can be attributed to two mechanisms. First, the formation of the capillary fringe zone (Fig. 1) ~~was formed~~ above the phreatic surface, ~~where~~ enabled the calculation of the Cap flux ~~was calculated~~. The Cap flux further contributed to the water loss that moved upward to the ~~ground~~ land surface, where E_{ss} takes place (Hird & Bolton, 2017; Balugani et al., 2021; 2023). Second, the improved simulation of $\psi_{s,i}$ and the corresponding θ created strong upward hydraulic gradients that promoted E_{ss} (Huo et

al., 2020). Both experimental (Huo et al., 2020) and field studies (Yang et al., 2021) have demonstrated that shallow groundwater, i.e. generally less than 2.5 m, can sustain evaporation by maintaining moisture supply to the soil layers.

4.3.2. Root soil water uptake

The inclusion of GWL as a dynamic bottom boundary had improved the simulation of the ~~soil matric potential (~~$\psi_{s,i}$~~) along~~ across the soil ~~layers~~ profile by allowing proper seasonal dynamics of $\psi_{s,i}$ with respect to ~~the position of~~ the GWL fluctuations. The improved representation of $\psi_{s,i}$ resulted in a substantial improvement of the RWU_s by better capturing the hydraulic connectivity between the saturated zone and the root zone (Wang et al., 2023). At Cabauw and Veenkampen, RWU_s, which is based on $\psi_{s,i}$ (Eq. 5), was increased by 29.6 and 35.9%, respectively. Such improvement highlights the sensitivity of the RWU_s to the groundwater depth, particularly when the groundwater depth lies within the range of 0.5 - 2.5 m from the land surface, as reported by Sulis et al. (2017). They demonstrated using two different models, i.e. TerrSysMP (Shrestha et al., 2014) and Parflow-WRF (Maxwell et al., 2011), applied at vegetated areas in the Rur catchment in Germany, that the GWL fluctuations significantly influence the energy fluxes, further affecting the RWU_s, through their impacts on the θ profile. This mechanism has been described by Huang et al. (2017) who showed that shallow groundwater can: a) prevent the ψ_l from declining to the critical ψ_l that trigger stomatal closure; and b) maintain high values of $\psi_{s,i}$, thereby preventing the rapid depletion of the θ. Consequently, these processes led to increasing the plant water storage and supported high RWU_s, as been observed in the ST-SC-MF6 simulations at Cabauw and Veenkampen sites.

4.3.3. Root groundwater uptake

~~Third, t~~The $\psi_{g,i}$ was explicitly defined ~~properly~~ for the soil layers below the capillary fringe zone, which was further used to calculate RWU_g (Eq. 6). The RWU_g is an additional component that contributed ~~-~~27.0, 15.2, 13.0% to the total ET at the ~~3~~ three sites (Loobos, Cabauw, and Veenkampen), respectively.

At Loobos, the maximum rooting depth of the evergreen forest was defined in the models as 4 m, allowing the plant roots to access the groundwater, located at depths between 3 and 5 m below the land surface. The increase in the RWU originated mainly from the RWU_g, while RWU_s showed nearly no change. That is because of the similar θ simulation by both ST-SC and ST-SC-MF6 models, resulting in comparable RWU_s estimates. Furthermore, the groundwater contribution to ET was more significant during dry periods (Figure 6b and c), when θ was depleted owing to lack of rains, while the GWL continued to support the water uptake by plant roots. Such mechanism has been reported in many previous studies (Zhu et al., 2009; Wang et al., 2023; Du et al., 2025). From a modelling perspective, Bieri et al. (2025) also showed that the failure of the models to reproduce proper dry season transpiration is often related to the absence of deep RWU mechanisms in the simulations. Moreover, the impacts of GT (discussed in Section 4.2.1) on cooling the T_s for the deeper soil layers, allowed for better RWU_g during spring and summer periods.

At Cabauw and Veenkampen, the maximum root depth of the grassland was set to 0.5 m in the models, allowing the roots to access the groundwater, fluctuated between 0 and 1.25 m below land surface. However, the contribution of RWU_g to the total ET at these two sites remained less as compared to Loobos. That is because the soil water availability, reflected in the improved simulation of θ by the ST-SC-MF6 models, was sufficient to sustain higher RWU_s, thereby reducing the reliance on the RWU_g. In such shallow water table conditions, land surface processes, including RWU, are subject to more energy control rather than water control (Wang et al., 2023).

~~4.3.~~4.4. Effect of groundwater on carbon fluxes and SIF

Explicit representation of groundwater in the IEM also had an impact on the carbon fluxes (GPP and NEE), particularly during dry periods (Ruehr et al., 2023), even though groundwater is not explicitly represented in the carbon fluxes' calculations. Instead, θ, which is dynamically constrained by GWL~~GWL~~, is included in the carbon fluxes' calculations and is positively correlated with carbon fluxes through affecting plant water status and stomatal conductance. When θ is limited (i.e., low

Formatte
Italic, Che

water content), both $\psi_{s,i}$ and ψ_l decreased (became more negative), and the gradient between the $\psi_{s,i}$ and ψ_l shifted to more negative. ~~With more negative ψ_l~~Under such conditions, the plant closed the stomata, so the stomatal conductance decreased in attempt to mitigate water stress, reducing CO_2 uptake and consequently lowering GPP and NEE. In contrast, higher θ increased the stomatal conductance, leading to higher CO_2 uptake, promoting carbon assimilation and higher GPP and NEE.

At Cabauw, where GWL is relatively shallow, exerting strong control on the θ dynamics, the ST-SC-M6 showed improved simulation of both θ and NEE, as compared to the ST-SC model. ~~Hence,~~In particular, the NEE was increased during the dry periods ~~at the Cabauw site~~ (Figure 7e and f~~Figs. 6e and f~~), due to ~~changes~~ enhancement in the simulated θ, resulting from the dynamically updated GWL values. This simulated mechanism aligns with recent findings that groundwater depth is a critical control on ecosystem productivity, with higher carbon assimilation occurring under shallow groundwater conditions (Glanville et al., 2023). Specifically, in meadow ecosystems with shallow GWL, such as in Cabauw, shallow groundwater can enhance net carbon uptake by suppressing soil respiration under near-saturated soil conditions, thereby increasing the net ecosystem carbon sink, as discussed by Sun et al. (2021). Their analysis, in two meadow sites in the Tibetan Plateau in China, revealed that the influence of high θ, maintained by shallow GWL, played a more significant role in controlling carbon fluxes rather than low temperature. Moreover, the pronounced improvement of the simulated NEE during the dry periods (Figure 7e and f) is consistent with the evidence that there is a significant positive correlation between groundwater depth and carbon fluxes under certain conditions, i.e. during dry periods when vegetation activity is minimum and carbon fluxes have low values (Koirala et al., 2017).

Meanwhile, at the Loobos site, there was ~~no~~negligible GWL effect on the simulated θ and consequently also on the simulated GPP ~~at the Loobos site~~ (Figure 7b and c). This is because: a) the simulated GWL was relatively moderate (3 – 5 m), limiting its hydraulic connection to the unsaturated zone, consistent with the observation that deeper GWL reduces carbon fluxes (Glanville

Formatte
Italic, Che

Formatte
Italic, Che

Formatte
Italic, Che

et al., 2023); and b) the maximum observed θ was generally low (0.16 m^3 m^{-3}), indicating low water availability for vegetation, and consequently poor carbon assimilation.

The contrasting responses between Loobos (no GPP improvement) and Cabauw (NEE improvement) demonstrate that groundwater effects on carbon cycling and vegetation productivity are strongly site dependent. Specifically, the groundwater influence becomes significant when the water table is shallow enough to interact with the root zone and meaningfully affect θ dynamics. These findings support recent calls to explicitly represent groundwater–carbon feedbacks in Earth system models to improve predictions of carbon fluxes under environmental change (Klaus, 2023). Moreover, it was highlighted by Tak et al. (2023) regarding the importance of groundwater level management to optimize ecosystem carbon uptake.

Similarly, ~~for~~ in the simulation of SIF, the impact of ~~the~~ groundwater ~~system~~ was evident at the Cabauw site through the changes in θ. The θ affects the water availability to the plant, which regulates the stomatal conductance and photosynthetic activity, and in turn contributes directly to the SIF calculations. The simulated SIF was enhanced in the dry summer days 9–14 August 2022 (~~Fig. 7a~~Figure 8a) due to the enhanced θ, caused by shallow GWL. Meanwhile, groundwater had no clear impact on the simulated θ during the summer days 3–6 June 2023 (~~Fig. 7c~~Figure 8c), since, during those days, both ST-SC and ST-SC-MF6 produced a very similar θ simulation (~~Figs. 5aa~~ Figure 4b and c), resulting in no groundwater impact on the SIF simulation. While both models underestimated the SIF on the winter days 12–15 November 2022 (~~Fig. 7b~~Figure 8b), likely due to other parameters and/or forces that could influence the SIF calculations, which are beyond the scope of this study and need further investigation.

Formatte
Italic, Che

~~4.4.~~4.5. Recommendations

The changes in the θ, T_s, ET, GPP, NEE, and SIF variables suggest that accounting for groundwater interactions significantly improves the model's ability to represent the SPAC. However, certain assumptions and/or limitations highlight areas for future development. The coupling between

STEMMUS-SCOPE and MODFLOW 6 was applied to three sites in the Netherlands, and only for 1D vertical flow. Future enhancements would include expanding the ST-SC-MF6 IEM to 2 or 3D scale and incorporating groundwater lateral flow and surface runoff. Furthermore, although calibration was performed manually in this proof-of-concept study, future work should incorporate a multi-objective automatic calibration framework to systematically reduce parameter uncertainty and enhance model robustness. Implementing such an approach in future 2D/3D applications will increase confidence in predictive simulations and strengthen the broader applicability of the developed IEM. Moreover, the inconsistency in the amplitude of the simulated T_s (i.e., higher peaks or lower troughs than observations) could be addressed by improving the boundary layer resistance scheme in STEMMUS-SCOPE. Additionally, the incorporation of a more physically based simulation of SIF is expected to better capture the SIF dynamics, especially during winter periods.

5. Conclusions

This study demonstrated the added value of incorporating the groundwater component in modelling the SPAC. To achieve this, an IEM framework was developed by coupling the STEMMUS-SCOPE SPAC model with the MODFLOW 6 IHM, resulting in the ST-SC-MF6 IEM. Results from three sites in the Netherlands (Loobos, Cabauw, and Veenkampen) demonstrate that explicitly including groundwater (mass and energy) in SPAC modelling improves the simulation of key ecohydrological variables, i.e. the θ dynamics, particularly at sites with shallow groundwater tables (Cabauw and Veenkampen) and during wet periods. This improved θ representation propagated to other processes, i.e. T_s dynamics, and ET components, including vegetation RWU. The enhanced ET simulation was realized at the three sites by improving the E_{ss} and the RWU_s simulations and by enabling the representation of Cap and RWU_g. In addition, groundwater – soil heat exchange improved the simulation of T_s profiles, further influenced energy partitioning and other T_s dependent processes, i.e. T_c, RWU and carbon uptake. Groundwater effects also propagated to ecosystem carbon

dynamics. At Cabauw, the improved θ enhanced stomatal conductance and carbon uptake, leading to improved simulations of NEE and SIF during dry conditions. In contrast, groundwater impacts on GPP were limited at Loobos, with limited specific retention capacity and relatively moderate groundwater depths, emphasizing that groundwater – vegetation interactions are strongly site dependent and controlled by groundwater depth, soil properties, and rooting characteristics. Overall, this study demonstrates that explicitly including groundwater dynamics with SPAC modelling is essential for realistically simulating ecosystem water, energy, and carbon cycles.~~This study demonstrated the added value of incorporating the groundwater component in modelling the soil-plant-atmosphere continuum. To achieve this, an IEM framework was developed by coupling the STEMMUS-SCOPE SPAC model with the MODFLOW 6 IHM, resulting in the ST-SC-MF6 IEM. The ST-SC-MF6 IEM was applied over an 8-year period (1 April 2016 – 31 March 2024) to 3 sites (Loobos, Cabauw, Veenkampen) located in the Netherlands. Conditions varied across the three sites, including depth to groundwater, soil characteristics, vegetation, and water management (e.g. the GWL at Cabauw is managed and the surroundings of Veenkampen were converted into wetlands since 2020). The results supported the hypothesis that explicit groundwater representation enhances the quantification of the soil-plant-atmosphere continuum. Both qualitative and quantitative results highlighted the improved performance of the ST-SC-MF6, as compared to the ST-SC in representing soil-plant-atmosphere continuum. The groundwater contribution was found to be spatially (contrasting the 3 study sites) and temporally variable. The groundwater impact was more pronounced at the sites with a shallower water table (Cabauw and Veenkampen), as compared to the Loobos site. Additionally, the groundwater effects on the final IEM solution were more pronounced during dry periods, when shallow groundwater continued to support vegetation to mitigate water stress. Having demonstrated the utility of including groundwater in an IEM, the tool can be used to study the cause-and-effect relationships in the soil-plant-atmosphere continuum that may be increasingly important during dry periods that wear-on, leading to lower water tables. In this study, explicit representation of groundwater in the IEM facilitated the influence of groundwater on

~~multiple soil and vegetation processes accomplished by: a) improving the simulation of the θ and T_s profiles, b) adding the RWU_g to the total ET, c) capturing the dynamics of the unsaturated and saturated zones by enabling dynamic exchange of the R_g, Cap, Q_{heat} fluxes and the GWL, GT, and RT_g variables between the two zones, and d) indirectly by refining the simulated θ and T_s profiles through better simulation of: i) the E and RWU_s, further both contribute to ET, ii) the carbon fluxes (GPP and NEE), and iii) the SIF. Overall, the findings of this study highlight the importance of the IEM framework for deepening the understanding of ecosystem functioning. Simply, including a more robust representation of groundwater in the ST-SC-MF6-IEM facilitated significant improvement in the simulated water, energy, and carbon cycles. Future work will address the current limitations (i.e., ignoring lateral groundwater flow and surface runoff, and simplifying the boundary layer resistance scheme and SIF simulation) that were not resolved in this study and might further improve the accuracy and applicability of the ST-SC-MF6-IEM.~~

Code availability

STEMMUS-SCOPE v.1.6.1 is available as open-source code repository at https://github.com/EcoExtreML/STEMMUS_SCOPE. STEMMUS-SCOPE was run using the PyStemmusScope v0.5.0 Python package available at https://github.com/EcoExtreML/STEMMUS_SCOPE_Processing.

MODFLOW 6 v.6.6.0 is available at https://www.usgs.gov/software/modflow-6-usgs-modular-hydrologic-model and as open-source code repository from https://github.com/MODFLOW-ORG/modflow6. MODFLOW 6 was run using the modflowapi v0.3.0 Python package available at https://github.com/MODFLOW-ORG/modflowapi.

Authors contribution

Conceptualization: MGD, YZ, CVT, MWL, MSS, ZBS

Data curation: MGD, PK, HZ, MVM

Formal analysis: YZ, LY

Funding acquisition: YZ, CVT, JS, ZBS

Methodology: All authors

Project administration: CVT

Software: MGD, FA, BS, ZS

Supervision: CVT, MWL, MSS

Visualization: MGD

Writing – original draft: MGD

Writing – review & editing: All authors

Competing interest

One of the co-authors (Zhongbo Su) is a member of the editorial board of the journal. Other authors declare that they have no conflict of interest.

Acknowledgements

The authors would like to acknowledge Guido Bakema from Wageningen Environmental Research for early discussions; David Berger, Michael Fienen, Geoffrey Moret, Sarah Peterson, and Kevin Jones from the U.S. Geological Survey for their review of the manuscript. We would also like to thank the Handling Editor Patricia Saco, the Reviewer Emmanuel Dubois, one Anonymous Reviewer and the Community Member Giacomo Medici for their constructive comments, which allowed us to improve the quality of the manuscript.

Any use of trade, firm, or product names is for descriptive purposes only and does not imply endorsement by the U.S. Government.

Financial support

This research was supported by the Faculty of Geo-Information Science and Earth Observation (ITC), University of Twente, the Netherlands. The authors would like to acknowledge the Netherlands eScience Center **EcoExtreML** project (grant no. 27020G07), the Netherlands Organization for Scientific Research (NWO) KIC **WUNDER** project (grant no. KICH1. LWV02.20.004), and the European Union's Horizon Europe research and innovation programme under Grant Agreement No 101156076, **DRYAD** project.

References

Agbotui, P. Y., Firouzbehi, F., & Medici, G. (2025). Review of Effective Porosity in Sandstone Aquifers: Insights for Representation of Contaminant Transport. *Sustainability*, *17*(14), 6469. https://doi.org/10.3390/su17146469

Akhter, T., Pokhrel, Y., Felfelani, F., Ducharne, A., Lo, M. H., & Reinecke, R. (2025). Implications of Lateral Groundwater Flow Across Varying Spatial Resolutions in Global Land Surface Modeling. *Water Resources Research*, *61*(7), e2024WR038523. https://doi.org/10.1029/2024WR038523

Alkhaier, F., Flerchinger, G. N., & Su, Z. (2012). Shallow groundwater effect on land surface temperature and surface energy balance under bare soil conditions: Modeling and description. *Hydrology and Earth System Sciences*, *16*(7), 1817–1831. https://doi.org/10.5194/hess-16-1817-2012

Atkins, J. W., Bohrer, G., Fahey, R. T., Hardiman, B. S., Morin, T. H., Stovall, A. E. L., Zimmerman, N., & Gough, C. M. (2018). Quantifying vegetation and canopy structural complexity from terrestrial LiDAR data using the forestr r package. *Methods in Ecology and Evolution*, *9*(10), 2057–2066. https://doi.org/10.1111/2041-210X.13061

Balugani, E., Lubczynski, M. W., & Metselaar, K. (2021). Evaporation Through a Dry Soil Layer: Column Experiments. *Water Resources Research*, *57*(8), e2020WR028286. https://doi.org/10.1029/2020WR028286

Balugani, E., Lubczynski, M. W., Metselaar, K., & Balugani, E. (2023). Lysimeter and In-situ Field Experiments to Study Soil Evaporation through a Dry Soil Layer under Semi-Arid Climate. *Water Resources Research*, e2022WR033878. https://doi.org/10.1029/2022WR033878

Balugani, E., Lubczynski, M. W., Reyes-Acosta, L., van der Tol, C., Francés, A. P., & Metselaar, K. (2017). Groundwater and unsaturated zone evaporation and transpiration in a semi-arid open woodland. *Journal of Hydrology*, *547*, 54–66. https://doi.org/10.1016/J.JHYDROL.2017.01.042

Bense, V. F., & Kurylyk, B. L. (2017). Tracking the Subsurface Signal of Decadal Climate Warming to Quantify Vertical Groundwater Flow Rates. *Geophysical Research Letters*, *44*(24), 12,244-12,253. https://doi.org/10.1002/2017GL076015

Benz, S. A., Irvine, D. J., Rau, G. C., Bayer, P., Menberg, K., Blum, P., Jamieson, R. C., Griebler, C., &

Kurylyk, B. L. (2024). Global groundwater warming due to climate change. *Nature Geoscience*, *17*(6), 545–551. https://doi.org/10.1038/s41561-024-01453-x

Bieri, C. A., Dominguez, F., Miguez-Macho, G., & Fan, Y. (2025). Implementing deep soil and dynamic root uptake in Noah-MP (v4.5): Impact on Amazon dry-season transpiration. *Geoscientific Model Development*, *18*(12), 3755–3779. https://doi.org/10.5194/gmd-18-3755-2025

Bojinski, S., Verstraete, M., Peterson, T. C., Richter, C., Simmons, A., & Zemp, M. (2014). The Concept of Essential Climate Variables in Support of Climate Research, Applications, and Policy. *Bulletin of the American Meteorological Society*, *95*(9), 1431–1443. https://doi.org/10.1175/BAMS-D-13-00047.1

Bosveld, F. C. (2020). *The Cabauw In-situ Observational Program 2000 - Present: Instruments, Calibrations and Set-up*. https://cdn.knmi.nl/knmi/pdf/bibliotheek/knmipubTR/TR384.pdf

Brakkee, E., Van Huijgevoort, M. H. J., & Bartholomeus, R. P. (2022). Improved understanding of regional groundwater drought development through time series modelling: The 2018-2019 drought in the Netherlands. *Hydrology and Earth System Sciences*, *26*(3), 551–569. https://doi.org/10.5194/HESS-26-551-2022

Brunner, P., & Simmons, C. T. (2012). HydroGeoSphere: A Fully Integrated, Physically Based Hydrological Model. *Ground Water*, *50*(2), 170–176. https://doi.org/10.1111/j.1745-6584.2011.00882.x

Buishand, A., Jilderda, R., & Wijngaard, J. (2010). *KNMI - Regional differences in the extreme rainfall climatology in the Netherlands*. https://www.knmi.nl/kennis-en-datacentrum/achtergrond/regional-differences-in-the-extreme-rainfall-climatology-in-the-netherlands

Camporese, M., Paniconi, C., Putti, M., & Orlandini, S. (2010). Surface-subsurface flow modeling with path-based runoff routing, boundary condition-based coupling, and assimilation of multisource

observation data. *Water Resources Research*, *46*(2), 2512. https://doi.org/10.1029/2008WR007536

Chen, M., Xue, Y., Xue, Y., Peng, J., Guo, J., & Liang, H. (2024). Assessing the effects of climate and human activity on vegetation change in Northern China. *Environmental Research*, *247*, 118233. https://doi.org/10.1016/J.ENVRES.2024.118233

Colombo, R., Julitta, T., Pacheco, J., Cogliati, S., Sabater, N., & van der Tol, C. (2024). *Technical Assistance for the Development of Ground based Systems for Long term measurements of Red and Far red Sun Induced chlorophyll Fluorescence (DEFLOX) CCN4*. https://www.jb-hyperspectral.com/research-field/

Dai, T., Dai, X., Lu, H., He, T., Li, W., Li, C., Huang, S., Huang, Y., Tong, C., Qu, G., Shan, Y., Liang, S., & Liu, D. (2024). The impact of climate change and human activities on the change in the net primary productivity of vegetation—taking Sichuan Province as an example. *Environmental Science and Pollution Research*, *31*(5), 7514–7532. https://doi.org/10.1007/S11356-023-31520-6

Daoud, M. G., Lubczynski, M. W., Zoltan, V., & Francés, A. P. (2022). Application of a novel cascade-routing and reinfiltration concept with a Voronoi unstructured grid in MODFLOW 6, for an assessment of surface-water/groundwater interactions in a hard-rock catchment (Sardon, Spain). *Hydrogeology Journal*, 1–27. https://doi.org/10.1007/S10040-021-02430-Z

Daoud, M. G., White, J. T., Morway, E. D., van der Tol, C., & Lubczynski, M. W. (2024). Remote sensing evapotranspiration in ensemble-based framework to enhance cascade routing and re-infiltration concept in integrated hydrological model applied to support decision making. *Journal of Hydrology*, *637*, 131411. https://doi.org/10.1016/J.JHYDROL.2024.131411

de Conto, T., Armston, J., & Dubayah, R. (2024). Characterizing the structural complexity of the Earth's forests with spaceborne lidar. *Nature Communications 2024 15:1*, *15*(1), 1–15.

https://doi.org/10.1038/s41467-024-52468-2

de Wit, A., Boogaard, H., Fumagalli, D., Janssen, S., Knapen, R., van Kraalingen, D., Supit, I., van der Wijngaart, R., & van Diepen, K. (2019). 25 years of the WOFOST cropping systems model. *Agricultural Systems*, *168*, 154–167. https://doi.org/10.1016/J.AGSY.2018.06.018

Dronova, I., & Taddeo, S. (2022). Remote sensing of phenology: Towards the comprehensive indicators of plant community dynamics from species to regional scales. *Journal of Ecology*, *110*(7), 1460–1484. https://doi.org/10.1111/1365-2745.13897

Du, S., Jiang, S., Ren, L., Cui, H., Zhu, Y., He, M., & Xu, C. Y. (2025). Incorporating plant access to groundwater in global root zone storage capacity estimate. *Agricultural and Forest Meteorology*, *374*(2), 110807. https://doi.org/10.1016/j.agrformet.2025.110807

Egidio, E., De Luca, D. A., & Lasagna, M. (2024). How groundwater temperature is affected by climate change: A systematic review. *Heliyon*, *10*(6), 2405–8440. https://doi.org/10.1016/j.heliyon.2024.e27762

Elrashidy, M. T., Ireson, A. M., & Razavi, S. (2023). On the optimal level of complexity for the representation of groundwater-dependent wetland systems in land surface models. *Hydrology and Earth System Sciences*, *27*(24), 4595–4608. https://doi.org/10.5194/HESS-27-4595-2023

Fatichi, S., Ivanov, V. Y., & Caporali, E. (2012). A mechanistic ecohydrological model to investigate complex interactions in cold and warm water-controlled environments: 1. Theoretical framework and plot-scale analysis. *Journal of Advances in Modeling Earth Systems*, *4*(2), 5002. https://doi.org/10.1029/2011MS000086

Gao, X., Bai, Y., Huo, Z., Xu, X., Huang, G., Xia, Y., & Steenhuis, T. S. (2017). Deficit irrigation enhances contribution of shallow groundwater to crop water consumption in arid area. *Agricultural Water Management*, *185*(3), 116–125. https://doi.org/10.1016/j.agwat.2017.02.012

Gasper, F., Goergen, K., Shrestha, P., Sulis, M., Rihani, J., Geimer, M., & Kollet, S. (2014).

Implementation and scaling of the fully coupled Terrestrial Systems Modeling Platform (TerrSysMP v1.0) in a massively parallel supercomputing environment - A case study on JUQUEEN (IBM Blue Gene/Q). *Geoscientific Model Development*, *7*(5), 2531–2543. https://doi.org/10.5194/GMD-7-2531-2014

GCOS. (2025). *Essential Climate Variables*. Global Climate Observing System. https://gcos.wmo.int/site/global-climate-observing-system-gcos/essential-climate-variables

GDN. (2024). *DINOloket - Data and Information of the Dutch Subsurface*. Geological Survey of the Netherlands. https://www.dinoloket.nl/ondergrondgegevens

Glanville, K., Sheldon, F., Butler, D., & Capon, S. (2023). Effects and significance of groundwater for vegetation: A systematic review. *Science of The Total Environment*, *875*(11), 162577. https://doi.org/10.1016/j.scitotenv.2023.162577

Golaz, J. C., Van Roekel, L. P., Zheng, X., Roberts, A. F., Wolfe, J. D., Lin, W., Bradley, A. M., Tang, Q., Maltrud, M. E., Forsyth, R. M., Zhang, C., Zhou, T., Zhang, K., Zender, C. S., Wu, M., Wang, H., Turner, A. K., Singh, B., Richter, J. H., … Bader, D. C. (2022). The DOE E3SM Model Version 2: Overview of the Physical Model and Initial Model Evaluation. *Journal of Advances in Modeling Earth Systems*, *14*(12), e2022MS003156. https://doi.org/10.1029/2022MS003156;WGROUP:STRING:PUBLICATION

Graham, D. N., & Butts, M. B. (2005). FLEXIBLE INTEGRATED WATERSHED MODELING WITH MIKE SHE. In *Watershed models, Eds. V. P. Singh & D. K. Frevert* (pp. 245-272 Taylor and Francis). https://citeseerx.ist.psu.edu/document?repid=rep1&type=pdf&doi=4e9c3b289c52f7ff21471d7c3e9f357e66378ec9

Guo, Y. (1992). *Simulation of water transport in the soil-plant-atmosphere system*. https://doi.org/10.31274/RTD-180813-9473

Gupta, H. V., Kling, H., Yilmaz, K. K., & Martinez, G. F. (2009). Decomposition of the mean squared

error and NSE performance criteria: Implications for improving hydrological modelling. *Journal of Hydrology*, *377*(1–2), 80–91. https://doi.org/10.1016/J.JHYDROL.2009.08.003

Heinen, M., Brouwer, F., Teuling, C., & Walvoort, D. J. J. (2021). *BOFEK2020 - Bodemfysische schematisatie van Nederland : update bodemfysische eenhedenkaart*. Wageningen Environmental Research. https://doi.org/10.18174/541544

Heusinkveld, B. G., Barten, J. G. M., Fry, J. L., van der Molen, M., Nursanto, R. M., Ronda, R. J., & Snellen, H. (2024). *MAQ-Observations v1.0: Veenkampen*. https://maq-observations.nl/

Hird, R., & Bolton, M. D. (2017). Clarification of capillary rise in dry sand. *Engineering Geology*, *230*, 77–83. https://doi.org/10.1016/j.enggeo.2017.09.023

Huang, C. W., Domec, J. C., Ward, E. J., Duman, T., Manoli, G., Parolari, A. J., & Katul, G. G. (2017). The effect of plant water storage on water fluxes within the coupled soil-plant system. *New Phytologist*, *213*(3), 1093–1106. https://doi.org/10.1111/nph.14273

Hughes, J. D., Langevin, C. D., & Banta, E. R. (2017). Documentation for the MODFLOW 6 framework. In *U.S. Geological Survey Techniques and Methods 6-A57*. https://doi.org/10.3133/tm6a57

Hughes, J. D., Russcher, M. J., Langevin, C. D., Morway, E. D., & McDonald, R. R. (2022). The MODFLOW Application Programming Interface for simulation control and software interoperability. *Environmental Modelling & Software*, *148*, 105257. https://doi.org/10.1016/J.ENVSOFT.2021.105257

Huo, S., Jin, M., Liang, X., Li, X., & Hao, H. (2020). Estimating impacts of water-table depth on groundwater evaporation and recharge using lysimeter measurement data and bromide tracer. *Hydrogeology Journal*, *28*(3), 955–971. https://doi.org/10.1007/s10040-019-02098-6

Hutton, E. W. h., Piper, M. D., & Tucker, G. E. (2020). The Basic Model Interface 2.0: A standard interface for coupling numerical models in the geosciences. *Journal of Open Source Software*, *5*(51), 2317. https://doi.org/10.21105/JOSS.02317

Ireson, A. M., van der Kamp, G., Nachshon, U., & Butler, A. P. (2013). Modeling Groundwater-Soil-Plant-Atmosphere Exchanges in Fractured Porous Media. *Procedia Environmental Sciences*, *19*, 321–330. https://doi.org/10.1016/J.PROENV.2013.06.037

Jansen, F. A., Jongen, H. J., Jacobs, C. M. J., Bosveld, F. C., Buzacott, A. J. V., Heusinkveld, B. G., Kruijt, B., van der Molen, M., Moors, E., Steeneveld, G. J., van der Tol, C., van der Velde, Y., Voortman, B., Uijlenhoet, R., & Teuling, A. J. (2023). Land Cover Control on the Drivers of Evaporation and Sensible Heat Fluxes: An Observation-Based Synthesis for the Netherlands. *Water Resources Research*, *59*(11), e2022WR034361. https://doi.org/10.1029/2022WR034361

Klaus, M. (2023). Decadal increase in groundwater inorganic carbon concentrations across Sweden. *Communications Earth & Environment*, *4*(1), 221-. https://doi.org/10.1038/s43247-023-00885-4

Kløve, B., Ala-Aho, P., Bertrand, G., Gurdak, J. J., Kupfersberger, H., Kværner, J., Muotka, T., Mykrä, H., Preda, E., Rossi, P., Uvo, C. B., Velasco, E., & Pulido-Velazquez, M. (2014). Climate change impacts on groundwater and dependent ecosystems. *Journal of Hydrology*, *518*(PB), 250–266. https://doi.org/10.1016/J.JHYDROL.2013.06.037

KNMI. (2024). *KNMI Data Platform*. https://dataplatform.knmi.nl/organization/knmi

Knoben, W. J. M., Freer, J. E., & Woods, R. A. (2019). Technical note: Inherent benchmark or not? Comparing Nash-Sutcliffe and Kling-Gupta efficiency scores. *Hydrology and Earth System Sciences*, *23*(10), 4323–4331. https://doi.org/10.5194/HESS-23-4323-2019

Koirala, S., Jung, M., Reichstein, M., de Graaf, I. E. M., Camps-Valls, G., Ichii, K., Papale, D., Ráduly, B., Schwalm, C. R., Tramontana, G., & Carvalhais, N. (2017). Global distribution of groundwater-vegetation spatial covariation. *Geophysical Research Letters*, *44*(9), 4134–4142. https://doi.org/10.1002/2017GL072885

Langevin, C. D., Hughes, J. D., Banta, E. R., Niswonger, R. G., Panday, S., & Provost, A. M. (2017).

1698 Documentation for the MODFLOW 6 Groundwater Flow Model. In *U.S. Geological Survey*
1699 *Techniques and Methods 6-A55*. https://doi.org/10.3133/tm6a55

1700 Langevin, C. D., Hughes, J. D., Provost, A. M., Russcher, M. J., & Panday, S. (2023). MODFLOW as a
1701 Configurable Multi-Model Hydrologic Simulator. *Groundwater*, *62*(1), 111–123.
1702 https://doi.org/10.1111/GWAT.13351

1703 Langevin, C. D., Provost, A. M., Panday, S., & Hughes, J. D. (2022). Documentation for the MODFLOW
1704 6 Groundwater Transport Model. In *U.S. Geological Survey Techniques and Methods 6-A61*.
1705 https://doi.org/10.3133/TM6A61

1706 Lawrence, D. M., Fisher, R. A., Koven, C. D., Oleson, K. W., Swenson, S. C., Bonan, G., Collier, N.,
1707 Ghimire, B., van Kampenhout, L., Kennedy, D., Kluzek, E., Lawrence, P. J., Li, F., Li, H.,
1708 Lombardozzi, D., Riley, W. J., Sacks, W. J., Shi, M., Vertenstein, M., … Zeng, X. (2019). The
1709 Community Land Model Version 5: Description of New Features, Benchmarking, and Impact of
1710 Forcing Uncertainty. *Journal of Advances in Modeling Earth Systems*, *11*(12), 4245–4287.
1711 https://doi.org/10.1029/2018MS001583

1712 Lekula, M., & Lubczynski, M. W. (2019). Use of remote sensing and long-term in-situ time-series data
1713 in an integrated hydrological model of the Central Kalahari Basin, Southern Africa.
1714 *Hydrogeology Journal*, *27*(5), 1541–1562. https://doi.org/10.1007/s10040-019-01954-9

1715 Li, X., Zhao, Y., Xiao, W., Yang, M., Shen, Y., & Min, L. (2017). Soil moisture dynamics and implications
1716 for irrigation of farmland with a deep groundwater table. *Agricultural Water Management*,
1717 *192*(1), 138–148. https://doi.org/10.1016/j.agwat.2017.07.003

1718 Liao, C., Leung, L. R., Fang, Y., Tesfa, T., & Negron-Juarez, R. (2025). Representing lateral
1719 groundwater flow from land to river in Earth system models. *Geoscientific Model Development*,
1720 *18*(14), 4601–4624. https://doi.org/10.5194/GMD-18-4601-2025

1721 Lubczynski, M. W. (2009). The hydrogeological role of trees in water-limited environments.

Hydrogeology Journal, *17*(1), 247–259. https://doi.org/10.1007/s10040-008-0357-3

Malik, M. S., Shukla, J. P., & Mishra, S. (2021). Effect of Groundwater Level on Soil Moisture, Soil Temperature and Surface Temperature. *Journal of the Indian Society of Remote Sensing*, *49*(9), 2143–2161. https://doi.org/10.1007/s12524-021-01379-6

Mandal, D., & Roy, T. (2024). Climate Change Impacts on Soil Erosion and Land Degradation. In *Advances in Global Change Research* (Vol. 78, pp. 139–161). Springer Science and Business Media B.V. https://doi.org/10.1007/978-981-99-7935-6_5

Marchionni, V., Daly, E., Manoli, G., Tapper, N. J., Walker, J. P., & Fatichi, S. (2020). Groundwater Buffers Drought Effects and Climate Variability in Urban Reserves. *Water Resources Research*, *56*(5), e2019WR026192. https://doi.org/10.1029/2019WR026192

Martínez-De La Torre, A., & Miguez-Macho, G. (2019). Groundwater influence on soil moisture memory and land-atmosphere fluxes in the Iberian Peninsula. *Hydrology and Earth System Sciences*, *23*(12), 4909–4932. https://doi.org/10.5194/HESS-23-4909-2019

Maxwell, R. M., Lundquist, J. K., Mirocha, J. D., Smith, S. G., Woodward, C. S., Tompson, A. F. B., Maxwell, R. M., Lundquist, J. K., Mirocha, J. D., Smith, S. G., Woodward, C. S., & Tompson, A. F. B. (2011). Development of a Coupled Groundwater–Atmosphere Model. *Monthly Weather Review*, *139*(1), 96–116. https://doi.org/10.1175/2010MWR3392.1

McMillan, H. K., & Srinivasan, M. S. (2015). Characteristics and controls of variability in soil moisture and groundwater in a headwater catchment. *Hydrology and Earth System Sciences*, *19*(4), 1767–1786. https://doi.org/10.5194/hess-19-1767-2015

Milly, P. C. D. (1982). Moisture and heat transport in hysteretic, inhomogeneous porous media: A matric head-based formulation and a numerical model. *Water Resources Research*, *18*(3), 489–498. https://doi.org/10.1029/WR018I003P00489

Morway, E. D., Provost, A. M., Langevin, C. D., Hughes, J. D., Russcher, M. J., Chen, C. Y., & Lin, Y. F. F.

(2025). A New Groundwater Energy Transport Model for the MODFLOW Hydrologic Simulator. *Groundwater*. https://doi.org/10.1111/GWAT.13470

Myneni, R., Knyazikhin, Y., & Park, T. (2021). MODIS/Terra+Aqua Leaf Area Index/FPAR 4-Day L4 Global 500m SIN Grid V061 [Data set]. In *NASA EOSDIS Land Processes DAAC*. https://doi.org/10.5067/MODIS/MCD15A3H.061

Oishy, M. N., Shemonty, N. A., Fatema, S. I., Mahbub, S., Mim, E. L., Hasan Raisa, M. B., & Anik, A. H. (2025). Unravelling the effects of climate change on the soil-plant-atmosphere interactions: A critical review. *Soil & Environmental Health*, *3*(1), 100130. https://doi.org/10.1016/j.seh.2025.100130

Otoo, N. G., Sutanudjaja, E. H., van Vliet, M. T. H., Schipper, A. M., & Bierkens, M. F. P. (2025). Mapping groundwater-dependent ecosystems using a high-resolution global groundwater model. *Hydrology and Earth System Sciences*, *29*(8), 2153–2165. https://doi.org/10.5194/hess-29-2153-2025

Pacheco-Labrador, J., Perez-Priego, O., El-Madany, T. S., Julitta, T., Rossini, M., Guan, J., Moreno, G., Carvalhais, N., Martín, M. P., Gonzalez-Cascon, R., Kolle, O., Reischtein, M., van der Tol, C., Carrara, A., Martini, D., Hammer, T. W., Moossen, H., & Migliavacca, M. (2019). Multiple-constraint inversion of SCOPE. Evaluating the potential of GPP and SIF for the retrieval of plant functional traits. *Remote Sensing of Environment*, *234*(18), 111362. https://doi.org/10.1016/j.rse.2019.111362

Parrales, L. G., Martínez-León, J., Beltrán, J. J., Sariago Curi, R. A., Morales Pascual, J., Merino-Martínez, E., & García Gil, A. (2026). Vertical Heat Transfer Through the Unsaturated Zone in an Urban Alluvial Aquifer and Its Influence on Shallow Geothermal Plumes. *Sustainability*, *18*(3), 1551. https://doi.org/10.3390/su18031551

Peckham, S. D., Hutton, E. W. H., & Norris, B. (2013). A component-based approach to integrated

modeling in the geosciences: The design of CSDMS. *Computers and Geosciences*, *53*, 3–12. https://doi.org/10.1016/j.cageo.2012.04.002

Qian, L., Yu, X., Zhang, Z., Wu, L., Fan, J., Xiang, Y., Chen, J., & Liu, X. (2024). Assessing and improving the high uncertainty of global gross primary productivity products based on deep learning under extreme climatic conditions. *Science of The Total Environment*, *957*(6237), 177344. https://doi.org/10.1016/j.scitotenv.2024.177344

Rammler, M., & Bertermann, D. (2025). Groundwater temperatures downstream from a large-scale geothermal collector system (LSC) in Bad Nauheim, Germany. *Grundwasser*, *30*(1), 37–48. https://doi.org/10.1007/s00767-024-00580-x

Ruehr, S., Girotto, M., Verfaillie, J. G., Baldocchi, D., Cabon, A., & Keenan, T. F. (2023). Ecosystem groundwater use enhances carbon assimilation and tree growth in a semi-arid Oak Savanna. *Agricultural and Forest Meteorology*, *342*, 109725. https://doi.org/10.1016/j.agrformet.2023.109725

Saccò, M., Mammola, S., Altermatt, F., Alther, R., Bolpagni, R., Brancelj, A., Brankovits, D., Fišer, C., Gerovasileiou, V., Griebler, C., Guareschi, S., Hose, G. C., Korbel, K., Lictevout, E., Malard, F., Martínez, A., Niemiller, M. L., Robertson, A., Tanalgo, K. C., … Reinecke, R. (2024). Groundwater is a hidden global keystone ecosystem. *Global Change Biology*, *30*(1), e17066. https://doi.org/10.1111/GCB.17066

Samuel, J. B., & Chakraborty, A. (2023). Integration of a Groundwater Model to the Noah Land Surface Model for Aquifer-Soil Interaction. *Journal of Advances in Modeling Earth Systems*, *15*(7), e2022MS003153. https://doi.org/10.1029/2022MS003153

Schilperoort, B. (2025). *Sharing MATLAB models with everyone*. Netherlands EScience Center. https://blog.esciencecenter.nl/sharing-matlab-models-with-everyone-499eaf0a2e9e

Senf, C. (2022). Seeing the System from Above: The Use and Potential of Remote Sensing for

Studying Ecosystem Dynamics. *Ecosystems*, *25*(8), 1719–1737. https://doi.org/10.1007/S10021-022-00777-2

Shi, S., Yang, P., & van der Tol, C. (2023). Spatial-temporal dynamics of land surface phenology over Africa for the period of 1982–2015. *Heliyon*, *9*(6), 16413. https://doi.org/10.1016/J.HELIYON.2023.E16413

Shrestha, P., Sulis, M., Masbou, M., Kollet, S., & Simmer, C. (2014). A Scale-Consistent Terrestrial Systems Modeling Platform Based on COSMO, CLM, and ParFlow. *Monthly Weather Review*, *142*(9), 3466–3483. https://doi.org/10.1175/MWR-D-14-00029.1

Sulis, M., Williams, J. L., Shrestha, P., Diederich, M., Simmer, C., Kollet, S. J., Maxwell, R. M., Sulis, M., Williams, J. L., Shrestha, P., Diederich, M., Simmer, C., Kollet, S. J., & Maxwell, R. M. (2017). Coupling Groundwater, Vegetation, and Atmospheric Processes: A Comparison of Two Integrated Models. *Journal of Hydrometeorology*, *18*(5), 1489–1511. https://doi.org/10.1175/JHM-D-16-0159.1

Sun, S., Che, T., Gentine, P., Chen, Q., Wang, L., Yan, Z., Chen, B., & Song, Z. (2021). Shallow groundwater inhibits soil respiration and favors carbon uptake in a wet alpine meadow ecosystem. *Agricultural and Forest Meteorology*, *297*(1), 108254. https://doi.org/10.1016/j.agrformet.2020.108254

Sun, Y., Gu, L., Wen, J., van der Tol, C., Porcar-Castell, A., Joiner, J., Chang, C. Y., Magney, T., Wang, L., Hu, L., Rascher, U., Zarco-Tejada, P., Barrett, C. B., Lai, J., Han, J., & Luo, Z. (2023). From remotely sensed solar-induced chlorophyll fluorescence to ecosystem structure, function, and service: Part I—Harnessing theory. *Global Change Biology*, *29*(11), 2926–2952. https://doi.org/10.1111/GCB.16634

Tak, D. B. Y., Vroom, R. J. E., Lexmond, R., Lamers, L. P. M., Robroek, B. J. . M., & Temmink, R. J. M. (2023). Water level and vegetation type control carbon fluxes in a newly-constructed soft-

sediment wetland. *Wetlands Ecology and Management 2023 31:4*, *31*(4), 583–594. https://doi.org/10.1007/s11273-023-09936-1

Tang, E., Zeng, Y., Wang, Y., Song, Z., Yu, D., Wu, H., Qiao, C., Van Der Tol, C., Du, L., & Su, Z. (2024). Understanding the effects of revegetated shrubs on fluxes of energy, water, and gross primary productivity in a desert steppe ecosystem using the STEMMUS-SCOPE model. *Biogeosciences*, *21*(4), 893–909. https://doi.org/10.5194/BG-21-893-2024

Thum, T., Caldararu, S., Engel, J., Kern, M., Pallandt, M., Schnur, R., Yu, L., & Zaehle, S. (2019). A new model of the coupled carbon, nitrogen, and phosphorus cycles in the terrestrial biosphere (QUINCY v1.0; revision 1996). *Geoscientific Model Development*, *12*(11), 4781–4802. https://doi.org/10.5194/gmd-12-4781-2019

TNO – GDN. (2023). *BRO GeoTOP v1.6.* TNO - Geological Survey of the Netherlands. https://www.dinoloket.nl/en/subsurface-models/map

TNO – GDN. (2024). *BRO REGIS II v2.2.2.* TNO - Geological Survey of the Netherlands. https://www.dinoloket.nl/en/subsurface-models/map

Van Cleemput, E., Adler, P. B., Suding, K. N., Rebelo, A. J., Poulter, B., & Dee, L. E. (2025). Scaling-up ecological understanding with remote sensing and causal inference. *Trends in Ecology and Evolution*, *40*(2), 122–135. https://doi.org/10.1016/J.TREE.2024.09.006

van Dam, J. C., Groenendijk, P., Hendriks, R. F. A., & Kroes, J. G. (2008). Advances of Modeling Water Flow in Variably Saturated Soils with SWAP. *Vadose Zone Journal*, *7*(2), 640–653. https://doi.org/10.2136/VZJ2007.0060

van der Molen, M., Barten, J. G. M., Snellen, H., Peters, W., & Vilà-Guerau de Arellano, J. (2024). *MAQ-Observations v1.0: Loobos*. https://maq-observations.nl/

Van Der Tol, C., Verhoef, W., Timmermans, J., Verhoef, A., & Su, Z. (2009). An integrated model of soil-canopy spectral radiances, photosynthesis, fluorescence, temperature and energy balance.

Biogeosciences, *6*(12), 3109–3129. https://doi.org/10.5194/BG-6-3109-2009

Van der Velde, R., Benninga, H. J. F., Retsios, B., Vermunt, P. C., & Salama, M. S. (2023). Twelve years of profile soil moisture and temperature measurements in Twente, the Netherlands. *Earth System Science Data*, *15*(4), 1889–1910. https://doi.org/10.5194/essd-15-1889-2023

Van Walsum, P. E. V., & Supit, I. (2012). Influence of ecohydrologic feedbacks from simulated crop growth on integrated regional hydrologic simulations under climate scenarios. *Hydrology and Earth System Sciences*, *16*(6), 1577–1593. https://doi.org/10.5194/HESS-16-1577-2012,

Wang, T., Wu, Z., Wang, P., Wu, T., Zhang, Y., Yin, J., Yu, J., Wang, H., Guan, X., Xu, H., Yan, D., & Yan, D. (2023). Plant-groundwater interactions in drylands: A review of current research and future perspectives. *Agricultural and Forest Meteorology*, *341*, 109636. https://doi.org/10.1016/j.agrformet.2023.109636

Wang, X., He, L., Li, P., Ma, J., Shi, Y., Tian, Q., Zhao, G., He, J., Feng, H., Shi, H., & Yu, Q. (2026). Spatially adaptive estimation of multi-layer soil temperature at a daily time-step across China during 2010–2020. *Earth System Science Data*, *18*(1), 97–116. https://doi.org/10.5194/essd-18-97-2026

Wang, Y., Zeng, Y., Yu, L., Yang, P., Van Der Tol, C., Yu, Q., Lü, X., Cai, H., & Su, Z. (2021). Integrated modeling of canopy photosynthesis, fluorescence, and the transfer of energy, mass, and momentum in the soil-plant-Atmosphere continuum (STEMMUS-SCOPE v1.0.0). *Geoscientific Model Development*, *14*(3), 1379–1407. https://doi.org/10.5194/GMD-14-1379-2021

Williams, M., Law, B. E., Anthoni, P. M., & Unsworth, M. H. (2001). Use of a simulation model and ecosystem flux data to examine carbon-water interactions in ponderosa pine. *Tree Physiology*, *21*(5), 287–298. https://doi.org/10.1093/TREEPHYS/21.5.287

Williams, M., Rastetter, E. B., Fernandes, D. N., Goulden, M. L., Wofsy, S. C., Shaver, G. R., Melillo, J. M., Munger, J. W., Fan, S. M., & Nadelhoffer, K. J. (1996). Modelling the soil-plant-atmosphere

continuum in a Quercus–Acer stand at Harvard Forest: the regulation of stomatal conductance by light, nitrogen and soil/plant hydraulic properties. *Plant, Cell & Environment*, *19*(8), 911–927. https://doi.org/10.1111/J.1365-3040.1996.TB00456.X

Xin, P., Yu, X., Zhan, L., Cheng, H., & Yuan, S. (2023). Surface water-groundwater interaction affects soil temperature distributions and variations in salt marshes. *Advances in Water Resources*, *172*, 104366. https://doi.org/10.1016/J.ADVWATRES.2023.104366

Yang, C., & Lei, H. (2024). Evaluation of data assimilation strategies on improving the performance of crop modeling based on a novel evapotranspiration assimilation framework. *Agricultural and Forest Meteorology*, *346*(11), 109882. https://doi.org/10.1016/j.agrformet.2023.109882

Yang, T., Ala, M., Guan, D., & Wang, A. (2021). The Effects of Groundwater Depth on the Soil Evaporation in Horqin Sandy Land, China. *Chinese Geographical Science*, *31*(4), 727–734. https://doi.org/10.1007/s11769-021-1220-x

Yang, X., Hu, J., Ma, R., & Sun, Z. (2021). Integrated Hydrologic Modelling of Groundwater-Surface Water Interactions in Cold Regions. *Frontiers in Earth Science*, *9*. https://doi.org/10.3389/FEART.2021.721009

Yu, L., Zeng, Y., Wen, J., & Su, Z. (2018). Liquid-Vapor-Air Flow in the Frozen Soil. *Journal of Geophysical Research: Atmospheres*, *123*(14), 7393–7415. https://doi.org/10.1029/2018JD028502

Zeng, J., Yang, J., Zha, Y., & Shi, L. (2019). Capturing soil-water and groundwater interactions with an iterative feedback coupling scheme: New HYDRUS package for MODFLOW. *Hydrology and Earth System Sciences*, *23*(2), 637–655. https://doi.org/10.5194/HESS-23-637-2019

Zeng, Y., Alidoost, F., Schilperoort, B., Liu, Y., Verhoeven, S., Grootes, M. W., Wang, Y., Song, Z., Yu, D., Tang, E., Han, Q., Yu, L., Daoud, M. G., Khanal, P., Chen, Y., van der Tol, C., Zurita-Milla, R., Girgin, S., Retsios, B., … Su, Z. (2025). Towards an open soil-plant digital twin based on

STEMMUS-SCOPE model following open science. *Computers & Geosciences*, *205*, 106013. https://doi.org/10.1016/J.CAGEO.2025.106013

Zeng, Y., & Su, Z. (2013). *STEMMUS : Simultaneous Transfer of Engery, Mass and Momentum in Unsaturated Soil*. University of Twente, Faculty of Geo-Information Science and Earth Observation (ITC). https://research.utwente.nl/en/publications/stemmus-simultaneous-transfer-of-engery-mass-and-momentum-in-unsa

Zeng, Y., Su, Z., Barmpadimos, I., Perrels, A., Poli, P., Boersma, K. F., Frey, A., Ma, X., de Bruin, K., Goosen, H., John, V. O., Roebeling, R., Schulz, J., & Timmermans, W. (2019). Towards a Traceable Climate Service: Assessment of Quality and Usability of Essential Climate Variables. *Remote Sensing*, *11*(10), 1186. https://doi.org/10.3390/RS11101186

Zeng, Y., Su, Z., Wan, L., & Wen, J. (2011a). A simulation analysis of the advective effect on evaporation using a two-phase heat and mass flow model. *Water Resources Research*, *47*(10). https://doi.org/10.1029/2011WR010701

Zeng, Y., Su, Z., Wan, L., & Wen, J. (2011b). Numerical analysis of air-water-heat flow in unsaturated soil: Is it necessary to consider airflow in land surface models? *Journal of Geophysical Research: Atmospheres*, *116*(D20), 20107. https://doi.org/10.1029/2011JD015835

Zhang, H., Xu, Y., & Kanyerere, T. (2020). A review of the managed aquifer recharge: Historical development, current situation and perspectives. *Physics and Chemistry of the Earth, Parts A/B/C*, *118–119*. https://doi.org/10.1016/j.pce.2020.102887

Zhao, H., Dolman, H., Elbers, J., Jans, W., Kruijt, B., Moors, E., Snellen, H., Vila-Guerau de Arellano, J., Peters, W., Krol, M. C., Hutjes, R., & van der Molen, M. (2026). The Loobos ecosystem first tower dataset: meteorology, turbulent fluxes and net ecosystem exchange (1996 to 2021). *Earth System Science Data*, *18*(3), 2023–2045. https://doi.org/10.5194/essd-18-2023-2026

Zhao, S., Zhao, X., Li, Y., Chen, X., Li, C., Fang, H., Li, W., & Guo, W. (2023). Impact of deeper

groundwater depth on vegetation and soil in semi-arid region of eastern China. *Frontiers in Plant Science*, *14*, 1186406. https://doi.org/10.3389/fpls.2023.1186406

Zhu, Y., Ren, L., Skaggs, T. H., Lü, H., Yu, Z., Wu, Y., & Fang, X. (2009). Simulation of Populus euphratica root uptake of groundwater in an arid woodland of the Ejina Basin, China. *Hydrological Processes*, *23*(17), 2460–2469. https://doi.org/10.1002/hyp.7353